2015

Distribution of Uranium in a Black Shale across the Shelf of the Late Pennsylvanian Midcontinent Sea

Maxwell A. Lindaman
Louisiana State University and Agricultural and Mechanical College

DISTRIBUTION OF URANIUM IN A BLACK SHALE ACROSS THE SHELF OF THE LATE PENNSYLVANIAN MIDCONTINENT SEA

A Thesis

Submitted to the Graduate Faculty of the
Louisiana State University and
Agricultural and Mechanical College
in partial fulfillment of the
requirements for the degree of
Master of Science

in

The Department of Geology and Geophysics

by
Maxwell A. Lindaman
B.S., Stony Brook University, 2012
December 2015

ACKNOWLEDGEMENTS

I'd like to thank my advisor Dr. Achim Herrmann for advice, funding, and the opportunity to work on this project. This gratitude is extended to my committee members, Dr. Carol Wicks and Dr. Huiming Bao, for their time and availability. Another thanks goes to Wanda LeBlanc for her generous assistance with XRD data collection and analysis, and to Adam Turner for providing important additional data. I'd also like to thank my family for their sustained encouragement and support of my education. A final acknowledgement goes to the friends that I've made over the course of my studies, who have helped make my time at LSU memorable and enjoyable.

TABLE OF CONTENTS

LIST OF TABLES

LIST OF FIGURES

ABSTRACT

Uranium paleoredox proxies such as enrichment factors and $^{238}U/^{235}U$ ratios can be used to reconstruct redox conditions in ancient water masses on local and global scales based on the differential behavior of uranium in oxic, suboxic, and anoxic environments. Many studies have focused on black shales due to their high levels of metal enrichment and association with climactic events. However, the influence of local effects on U accumulation is uncertain, particularly in ancient epeiric sea environments.

This study consists of two parts: an evaluation of common sequential extraction methods for U analysis (particularly the Tessier-type sequential extraction) and the application of a modified procedure to study the U distribution in samples of the Heebner shale of the Late Pennsylvanian Midcontinent Sea. XRD data were collected to evaluate the effects of the extractions on relevant minerals and to supplement the U concentration data for the Heebner samples. Nitrogen isotope excursions that are present in each of the studied outcrops were used for geochemical horizon correlation.

The results suggest that sequential extractions can aid in the successful application of U paleoredox proxies, but additional modifications may be required to common extraction procedures. These modifications include steps that better isolate organic matter and apatite. The results of a sequential extraction on the Heebner indicate that U is largely partitioned between apatite and fractions that are loosely associated with organic matter, although the true associations of U with organic matter are unclear. Apatite condensation surfaces occur predictably and are likely caused by redox cycling in the water column. This may negatively affect uranium redox proxies due to the association of U-enriched apatite with fluctuating rather than persistently anoxic conditions in the water column. The spatial variation in U and apatite accumulation at the three outcrop locations supports the prevailing superestuarine circulation model for black shale deposition in the LPMS, but does not support the hypothesis that an upwelling belt occurred in the Southern area of the Midcontinent shelf.

INTRODUCTION

Uranium enrichment factors and $^{238}U/^{235}U$ ratios have been used as paleoredox proxies in a number of studies (e.g. Hatch & Leventhal 1992, Hoffman et al. 1998, Algeo & Maynard 2004, Schröder & Grotzinger 2007, Algeo & Tribovillard 2009, Chun et al. 2010, Montoya-Pino et al. 2010, Brennecka et al. 2011, Tribovillard et al. 2012, Asael et al. 2013, Kendall et al. 2013, Partin et al. 2013, Dahl et al. 2014, Lash & Blood 2014, Kendall et al. 2015). Under anoxic conditions, U is reduced from a mobile hexavalent state to a particle-reactive tetravalent state (Anderson 1989, Barnes & Cochran 1990, Klinkhammer & Palmer 1991, Ivanovich & Harmon 1992, Swarzenski et al. 1999). As a result of this transition, reducing sediments are often associated with enhanced U accumulation as well as an isotopic fractionation that favors the heavier (U^{238}) isotope (Weyer et al. 2008, Murphy et al. 2013, Andersen et al. 2014, Holmden et al. 2015, Noordman et al. 2015, Stylo et al. 2015). Although there is a general association between reducing conditions and U accumulation and $^{238}U/^{235}U$ fractionation, there are several effects that have the potential to complicate this relationship. U accumulation rates are known to be affected by variables such as sedimentation rate (Lüning & Kolonic 2003), oxygen penetration depth (Zheng et al. 2002, McManus et al. 2005, Zhang et al. 2011), reservoir effects (Anderson et al. 1989, Algeo & Tribovillard 2009, Andersen et al. 2014), and organic matter content and flux (Spirakis 1996, Lüning & Kolonic 2003, McManus et al. 2005, Chermak & Schreiber 2014). Uranium-based paleoredox studies have often focused on sediments deposited under reducing environments such as black shales (e.g. Algeo & Tribovillard 2009, Montoya-Pino et al. 2010, Asael et al. 2013, Kendall et al. 2013) because they are typically enriched in trace metals (Piper & Calvert 2009) and are associated with climactic perturbations (Kolonic et al. 2005, Bonis & Kürschner 2010, Montoya-Pino et al. 2010).

One challenge involved with the study of black shale deposits is that ancient environments of deposition such as epeiric seas do not have modern equivalents (Arthur & Sageman 1994, Algeo & Heckel 2008), and so the processes acting within them are more difficult to constrain. The extent to which local differences in lithology and water mass properties influence uranium accumulation in ancient black shale-producing environments is unclear, and so the application of U enrichment factors and $^{238}U/^{235}U$ proxies may be complicated.

A potential method to improve the applicability of U-based paleoredox techniques in epeiric sea black shale is sequential extraction, where a sample undergoes a series of chemical extractions to determine the particulate associations of its trace metals. This method identifies U-bearing constituents in the sample and quantifies their relative importance, which can illuminate locally-acting processes that influence U accumulation or isotopic composition. Spatial variations can also be established if multiple samples at different locations are analyzed. In this manner U paleoredox proxies can be improved by studying the resultant gradients to determine the degree to which local effects (as opposed to more general systemic redox conditions) are responsible for the observed trends.

Common sequential extraction methods such as the method of Tessier et al. (1979) and the BCR method (Quevaviller et al. 1997) may not be suitable for epeiric sea black shale. These methods do not have a step to isolate apatite minerals (which may be U-enriched) and contain an extraction for Fe and Mn oxides which may not be necessary. In this study, the Tessier-type sequential extraction method of Galindo et al. (2007) was evaluated for its effect on materials that are representative of black shale from the Late Pennsylvanian Midcontinent Sea (LPMS), an epeiric sea that covered a sizeable portion of the present interior of the United States. The procedure of Galindo et al. (2007) was chosen since it was used to study uranium distribution in a black shale, albeit a different type (the Timahdit shale of Morocco). This provided a base by which to compare and make adjustments.

A second sequential extraction was modified from this procedure to better isolate apatite minerals, which are commonly present in phosphatic nodules and known to be U-enriched (Runnels et al. 1953, Hoffman et al. 1998, Doveton & Merriam 2004). This second modified procedure was applied to samples from the Heebner shale at three outcrop locations across the shelf of the LPMS, and the extracts were analyzed for U concentrations. This work was complemented by bulk XRD analysis and nitrogen isotope data, the latter of which were used as a geochemical horizon correlation tool based on $\delta^{15}N$ excursions present at all three outcrops.

CHAPTER 1: BACKGROUND INFORMATION

1.1 CYCLOTHEMS AND THE LATE PENNSYLVANIAN MIDCONTINENT SEA

The primary samples of this study are from outcrops of black shale that was deposited in the Late Pennsylvanian Midcontinent Sea (LPMS), a large (~2.1 x 106 km^2) epeiric sea that covered a vast area of what is now the interior of the United States (Algeo & Heckel 2008, Figure 1). The black shales of the LPMS make good study units given their unique character, correlative outcrops, and an abundance of pre-existing studies.

Waxing and waning of Gondwanan ice sheets led to eustatic fluctuations that periodically flooded the cratonic interior (Heckel 2005). This led to the cyclic deposition of paleosols, coals, limestones, gray shales, and black shales. These successions are referred to as "cyclothems", and encompass glacial-interglacial cycles of approximately 10^5 years (Heckel 2008). The precise order of these units is variable and depends on location. An idealized *Kansas-type* cyclothem as described by Heckel (1977) begins with a transgressive limestone, which is overlain by a black shale that transitions into a grey shale (the "core shale"). These are followed by a regressive limestone and a terrestrial or nearshore "outside" shale to complete the cycle (Figure 2).

Like other epeiric seas of the past, the depositional environment of the LPMS does not have a precise modern equivalent. Modern epeiric seas such as the Baltic Sea and Hudson Bay are smaller and either oxic or intermittently oxic (Algeo & Heckel 2008), while the extensive black shale units of the LPMS are indicative of reducing conditions. Modern black-shale producing systems mainly consist of upwelling systems and restricted basins (Figure 3). These end members are not always adequate to describe the style of black shale deposition in epeiric seas (Arthur & Sageman 2004, Algeo & Heckel 2008). The upwelling model tends to create patchy deposits that are concentrated along a band below the upwelling zone. In the restricted basin model, trace element enrichments often exhibit gradual depletion or signatures that reflect restricted water mass renewal (Algeo & Tribovillard 2009). Paleogeographic reconstructions and temporal trace metal trends suggest that the LPMS had an unrestricted connection to the open ocean (Algeo & Heckel 2008, Algeo & Tribovillard 2009), which precludes the restricted basin model. The laterally extensive deposition of thin black shale in the LPMS suggests that the upwelling model is also not consummately applicable. Consequently, it is important to consider the unique paleoceanography that led to these deposits and how it may have influenced geochemical trends. This holds true for a number of techniques and proxies, including uranium-based methods.

The deposition of cyclothem black shales are best explained by a superestuarine circulation model (Heckel 1977, Algeo & Heckel 2008), where preconditioned oxygen-deficient deep water from the open ocean was advected into the LPMS in tandem with the formation of a halocline that was created by freshwater runoff during times of wetter climate (Figure 4). This may have graded into a thermocline in paleo-South of the LPMS, which maintained black shale deposition away from the runoff-induced halocline (Algeo & Heckel 2008).

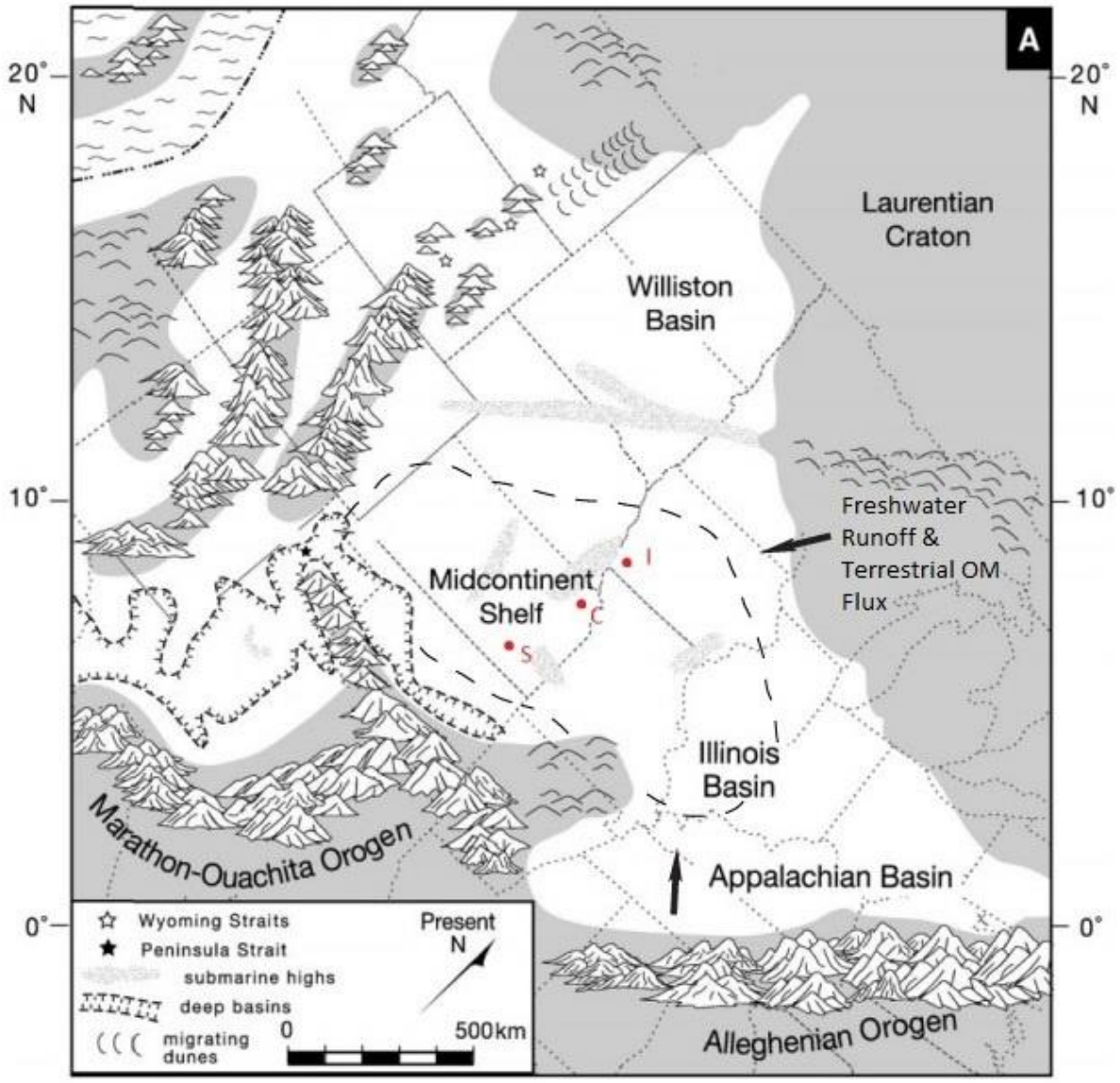

Figure 1: A paleogeographic reconstruction of the Late Pennsylvanian Midcontinent Sea, modified from Algeo & Heckel (2008), with present day state lines indicated. The approximate location of the three outcrops used in this study are marked with red dots (S = Sedan outcrop, C = Clinton outcrop, I = I229 outcrop), and the dashed lines are the approximate depositional extent of the study unit (the Heebner black shale, extent from Yang et al. 2003).

The end result was vertical stratification and oxygen-depleted bottom water, despite an unrestricted connection to the open ocean (Algeo & Maynard 2008). This general model is still debated; for example, recent work based on conodont $\delta^{18}O$ variations across the LPMS has suggested that the salinity gradient was pronounced only in the eastern most area of the sea near the Appalachian basin (Joachimski & Lambert 2015), with the implication that a halocline is not required for black shale deposition across the LPMS.

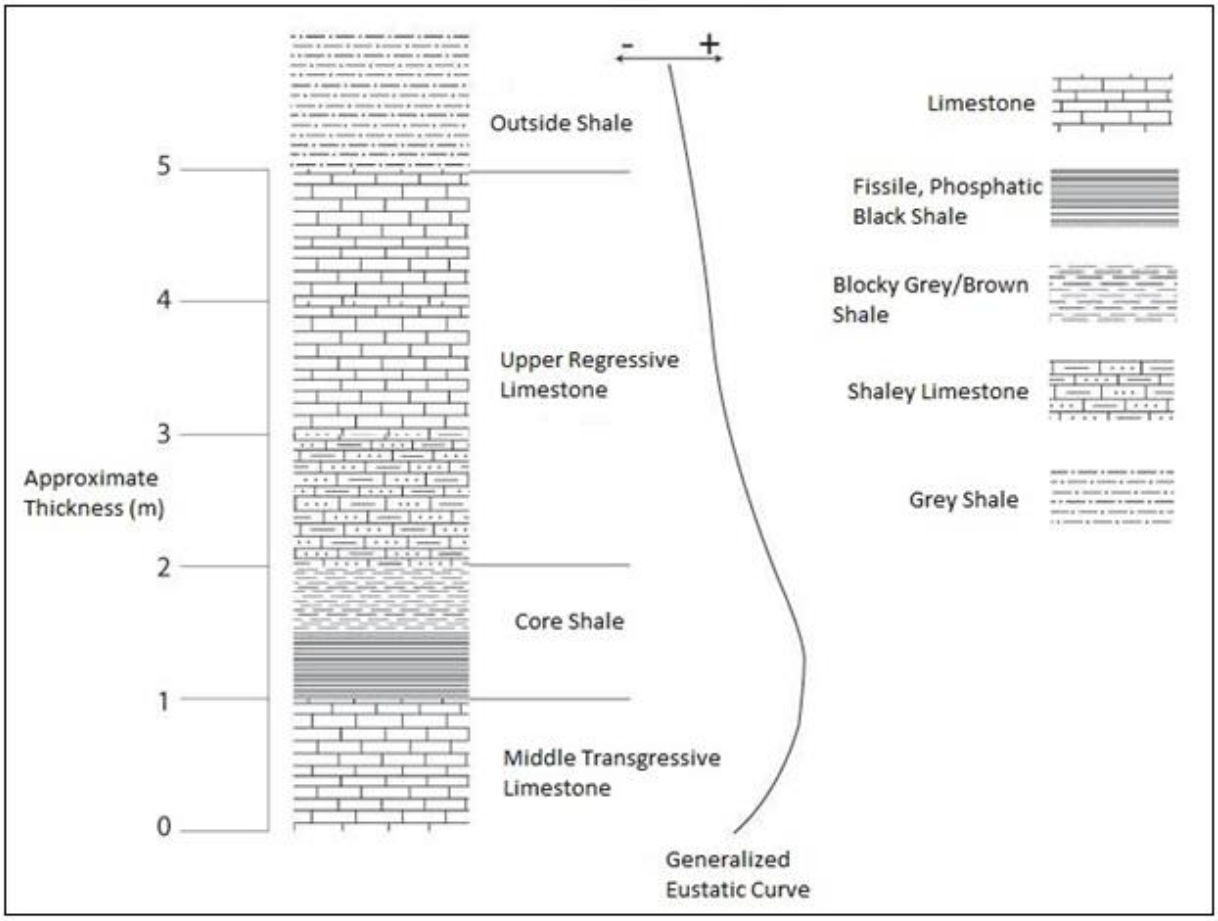

Figure 2: A generalized stratigraphic column for an idealized Kansas-type cyclothem with average thicknesses for each unit and a generalized eustatic curve, modified from Heckel (1977) and Algeo & Heckel (2008). The overarching control on the Kansas-type cyclothem sequence is considered to be eustatic rather than tectonic (Willard 1989, Heckel 1994). The "core shale" is composed of a lower phosphatic fissile black shale and an upper gray-brown shale. The upper regressive and middle transgressive limestones are skeletal calcilutites with marine biota, while the "outside" shale is typically non-marine with sparse fossils (Heckel 1977). Here the black shale is represented as a marine highstand deposit; other authors suggest a shallower water depth in relation to eustatic cycles (Zangerl & Richardson 1963, Coveney et al. 1991, Cecil et al. 2003).

For the LPMS to develop a superestuarine circulation cell, the water depth across the system would need to be deep enough to maintain a pycnocline (Heckel 1977). The black shales are generally taken to reflect open marine highstand conditions with restricted vertical circulation (Heckel 2005), but the water depth required for black shale deposition has been a contentious detail.

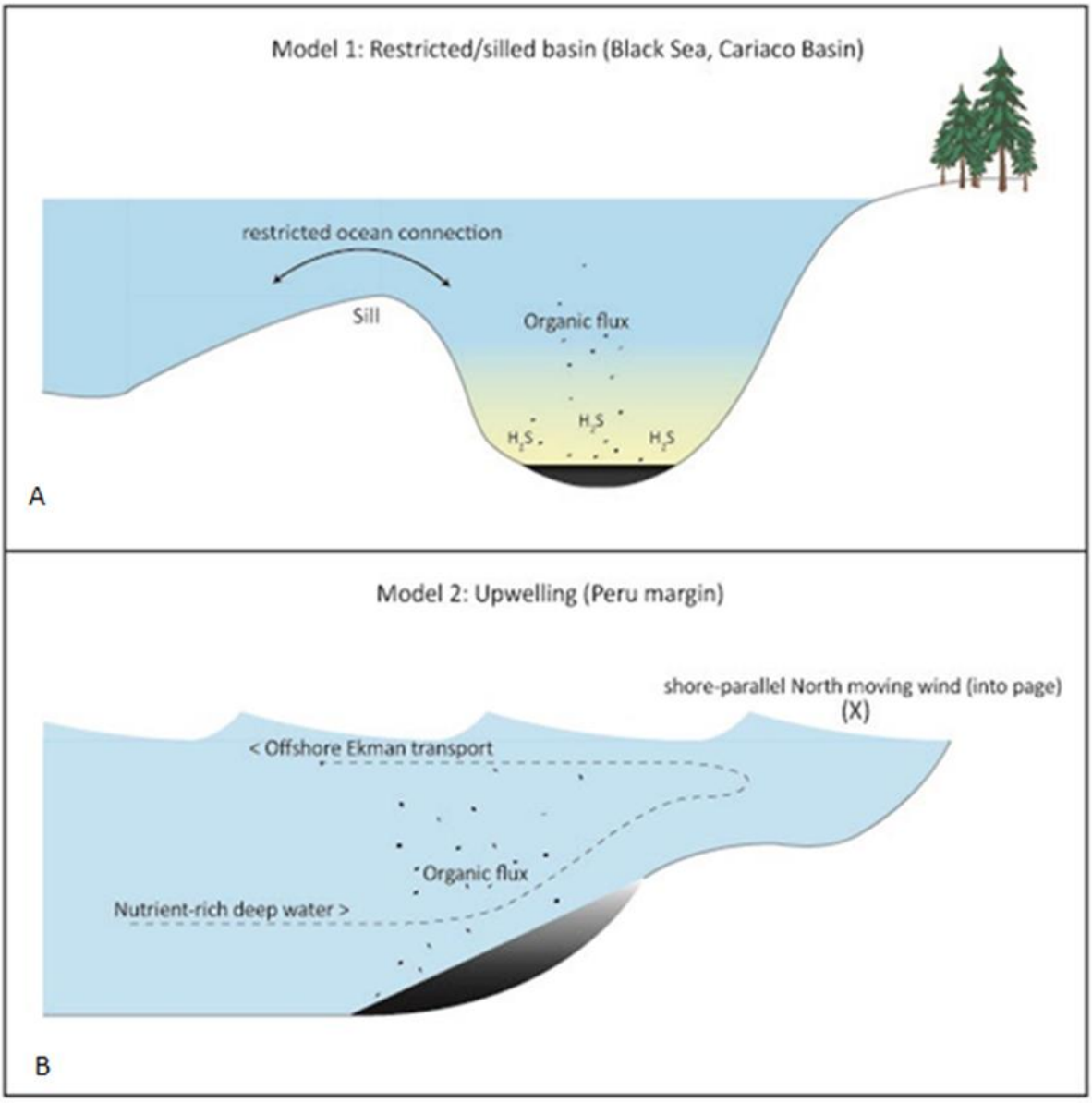

Figure 3: Modern depositional environments of black shale. In Model 1 (A), a submarine sill prevents the renewal of the bottom water in the basin, which leads to the development of oxygen-depleted (possibly sulfidic) conditions and the preservation of OM. In Model 2 (B), nutrient-rich deep water replaces surface water that is displaced by Ekman transport as a net result of shore-parallel winds and the Coriolis effect. Marine organic matter accumulates due to enhanced primary productivity in the nutrient rich-upwelled water.

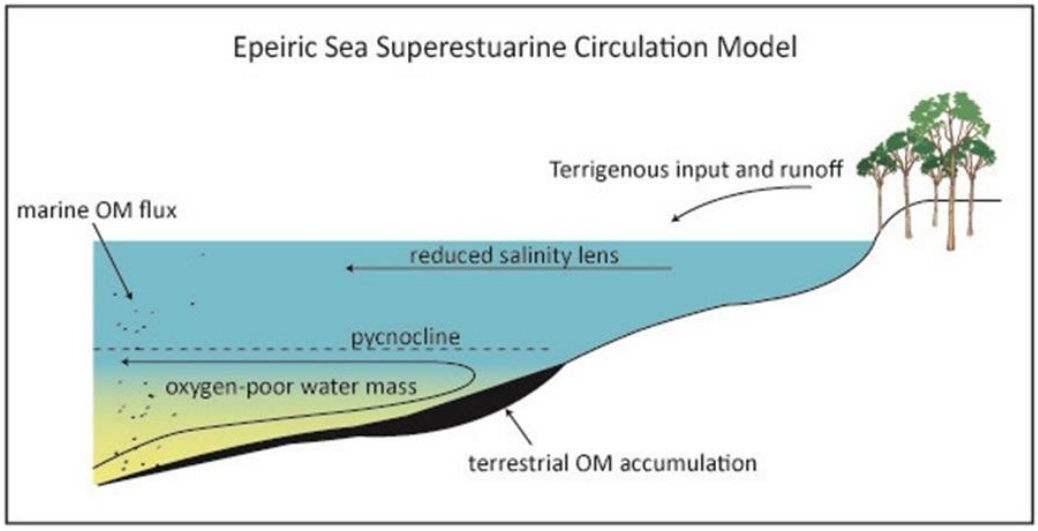

Figure 4: The superestuarine circulation model (Heckel 1977, Algeo & Heckel 2008) that has been used to explain the extensive deposition of thin black shales in the LPMS. In this model, preconditioned oxygen-poor deep water enters the system, and vertical mixing is prevented by the formation of a pycnocline (halocline) in as a result of freshwater runoff into the system. In the case of the LPMS, terrestrial OM accumulates in the nearshore region due to proximity to coal swamps, and marine OM increases in more distal settings.

Early work described the juxtaposition of black shale and coal in the Illinois basin (see Figure 1), which implies shallow water deposition (Zangerl 1963). Although some authors continue to argue for a general shallow water model (Cecil et al. 2014), the prevailing line of thought is that water depths were approximately ~100m (Heckel 2008). This inference is supported by a number of studies that demonstrate sea level fluctuations of 70-100m during cyclothem deposition, such as oxygen isotopes in brachiopods (Adlis et al. 1988), depositional topography of cyclothem carbonates (Soreghan and Giles 1999), and conodont oxygen isotopes (Joachimski et al. 2006). Egenhoff et al. (2012) suggested that some Pennsylvanian shales (including the Heebner shale of this study) were deposited within the photic zone due to evidence of microbial mats. The possibility remains that there were variable water depths across the LPMS that produced black shale concurrently; for example, Heckel (2005) attributed the juxtaposition of coal and black shale in the Illinois basin to a topographic high. It can be ascertained that the Midcontinent shelf of the LPMS was mostly flat and susceptible to rapid and extensive flooding when sea level rose (Cecil et al. 2014), which is evidenced by sharp lithological transitions (Yang et al. 2003) and a rapid movement of the chemocline across the shelf (Herrmann et al. 2015).

The stratification of the water column described by the superestuarine circulation provides a “preservation” mechanism. Preservation of organic matter (OM) is one requirement for the high OM content that defines black shale. The other requirements are productivity (or a source for the OM) and sedimentation rate, which governs whether the OM is diluted to the

point where the rock type is classified as a “normal” shale (Arthur & Sageman 1994). Primary (marine algal) productivity and sedimentation rates during black shale deposition in the LPMS are considered to have been generally low (Algeo & Heckel 2008). However, there was a high export of terrestrial OM from bordering coal swamps. This is reflected in the presence of large amounts of terrestrial organic macerals in some units (Schultz & Coveney 1992, Hoffman et al. 1998, Algeo et al. 2004, Algeo & Heckel 2008, Algeo et al. 2008). TOC generally increases towards the North/Northeast (paleo-direction), and this appears to be related to an increased flux of terrestrial organics from this direction (Coveney et al. 1987, Schultz & Coveney 1992, Hatch & Leventhal 1992). At the same time, redox-sensitive trace metal enrichment also increases towards the North/Northeast (Coveney et al. 1991, Schultz & Coveney 1992, Algeo et al. 1997, Hoffman et al. 1998, Cruse and Lyons 2004, Herrmann et al. 2015). Uranium and redox sensitive trace metal accumulation is heavily influenced by presence and flux of OM; its degradation consumes oxygen (Arndt et al. 2013), which helps to establish reducing conditions, and metal fixation in the sediment is promoted by the formation of organometallic ligands (Tribovillard et al. 2006). Additionally, the P released from decaying OM can lead to the precipitation of authigenic apatite (Ruttenberg & Berner 1993), which is often U-enriched (Soudry et al. 2002).

The increase in terrestrial OM is linked to freshwater flux (Algeo et al. 2004), and should designate areas where the halocline was strongest. This is one possible explanation for the trace element gradient that has been noted (paleo-North/Northeast nearshore-enriched). Another possibility that has been suggested is that the humic-rich organic matter of acidic nearshore environments is more conducive to trace metal enrichment (Coveney et al. 1991, Wignall & Maynard 1993). Schovsbo (2002) also suggested that some nearshore environments may have greater circulation and renewal of bottom waters due to current action, which could enhance uranium diffusion rates across the sediment-water interface. In order to address these issues, it is first required that the geochemical associations of U are identified and quantified across the system. Sequential extractions provide a means to accomplish these goals.

1.2 SEQUENTIAL EXTRACTIONS

Due to the uncertainties regarding the action of local effects and lithological changes on patterns of uranium accumulation in the LPMS, a method needed to be employed to describe U distribution in synchronous intervals across the larger depositional environment. A chemical sequential extraction was chosen as it allows for a more detailed analysis of a sample comparative to a bulk digest. Sequential extractions are procedures that use a series of chemical leaching steps to release one or more analytes from operationally defined fractions. The most common use of these procedures is to characterize the distribution of trace metals in soils and sediments (e.g. Ruttenberg 1992, Wenzel et al 2001, Quejido et al. 2005, Alvarez et al. 2014, Phan et al. 2015). Two sequential extraction methods have become standard procedures – the Tessier method (Tessier et al. 1979) and the BCR method (Quevaviller et al. 1997). They are similar in terms of reagent choice and the order of the extractions.

Two different sequential extractions were tested in this study: a more "standard" extraction (modified from Galindo et al. 2007) and a second extraction that was created for application to phosphatic black shales. The procedure modified from Galindo et al. (2007) was tested on several relevant materials for evaluative purposes, while the second procedure was tested on black shale samples from three outcrops to form a geochemical transect across the LPMS. The usefulness of any extraction procedure is dependent on the sample composition and the chemical behavior of the analyte. When sequential extractions are used as a tool to precisely identify the geochemical associations of trace metals, the results are subject to additional scrutiny regarding specificity, and modifications to the more common procedures may be required. The issue of specificity has been the feature of numerous revisions and evaluations of sequential extraction methods (e.g. Usero et al. 1998, Rauret et al. 1999, Mossop et al. 2003, Bacon et al. 2005, Arain et al. 2009, Okoro et al. 2012). In the case of this study, the sequential extraction creates a more nuanced picture of sample composition and spatiotemporal gradients by partitioning the analyte (uranium) into operationally defined fractions.

1.3 STUDY UNIT AND DEPOSITIONAL ENVIRONMENT

The primary sample set of this study was from the Heebner shale of the Shawnee group of the Oread cyclothem. The Oread cyclothem consists of alternating shale and limestone, and outcrops at several locations in the Midcontinent along with other upper Pennsylvanian strata. The Heebner shale is about 2 meters thick and can be subdivided into a lower and upper part similar to other Kansas-type core shales (Figure 2). The lower part is more fissile and consists of brownish-black claystone, and the upper part is a semi-fissile olive-brown siltstone. In southeastern Kansas, a thin gray shale sits below the lower fissile black claystone (Yang et al. 2003). Phosphatic nodules and lamina are common in the lower fissile half.

The Heebner shale was deposited on the continental shelf of the LPMS during marine highstand (Figure 1). In Northern Oklahoma, it thickens abruptly into diverse prodeltaic deposits that are 10-30m thick (Yang et al. 2003). The clastic flux that built these deltas was provided by erosion of the Ouachita Mountains, which was enhanced by renewed uplift and generally wet conditions at the time of deposition (Yang et al. 2003). The shale maintains a nearly constant thickness across the shelf and exhibits sharp upper, lower, and intra-layer contacts, which indicates rapid transitions in depositional conditions across large areas (Yang et al. 2003). This supports the notion of low relief across the shelf (Cecil et al. 2014, Herrmann et al. 2015).

Yang et al. (2003) proposed a model to explain the abrupt juxtaposition of deltaic and anoxic black shale facies of the Heebner shale along with and the steepness of the prodeltaic slopes in Northern Oklahoma. Their model is a refined version of the Heckel (1977) model, which attributes shelf anoxia to both super-estuarine circulation and upwelling along the southern margin of the system. Yang et al. (2003) used the Northwest African upwelling system as an analogue to determine that an upwelling belt may have occurred north of the southern coast (paleo-direction) of the Kansas shelf due to Ekman transport. The inferred direction of the

trade wind (Heckel 1977) suggests that a clockwise surface water circulation pattern would have occurred in the LPMS, which moved west across the southern margin of the system between the shoreline and the upwelling center (Yang et al. 2003).

Geochemically and compositionally, the Heebner shale has been described as an "offshore marine" endmember of the Pennsylvanian black shales, with a relatively large amount of marine organic matter and greater phosphate content compared to the nearshore shales of the paleo-North/Northeast (Schultz & Coveney 1992). In contrast, the nearshore shales of the southern margin in Kansas and Southeastern Nebraska have less trace metal enrichment and contain less organic matter, possibly due to siliciclastic dilution (Yang et al. 2003, Schultz & Coveney 1992).

CHAPTER 2: MATERIALS AND METHODS

2.1 STANDARD SEQUENTIAL EXTRACTION EVALUATION

Several materials were tested to evaluate the effectiveness of a typical sequential extraction on materials relevant to the LPMS black shales. The procedure that was used was modified from Galindo et al. (2007) and shown in Table 1.

Table 1: A "standard" sequential extraction, modified from Galindo et al. 2007

Extraction Step	Target material/objective	Reagent	Reaction/agitation time and parameters
F1	Exchangeable	25 mL 1M $MgCl_2$	24hrs at 25°C
F2	Carbonates	35 mL 1M CH_3COONa + 1M CH_3COOH	24hrs at 25°C
F3	Fe/Mn oxides	0.04M $NH_2OH{\cdot}HCl$ + 25% v/v 1M CH_3COOH pH=2 (adjusted with HNO_3)	24hrs at 25°C
F4.1	Organic matter/pyrite	25 mL H_2O_2 + 15 mL 0.02M HNO_3	2hrs at 85°C
F4.2	Organic matter/pyrite	15 mL H_2O_2 + 9 mL 0.02M HNO_3	3hrs at 85°C
F4.3	Prevention of re-adsorption of analyte	35mL 3.2M CH_3COONa in 20% HNO_3	0.5hrs at 25°C
F5	Residual material	20mL aqua regia	14hrs at 90°C

The tested materials were the following: an analogous black shale from a Permian cyclothem, a USGS shale standard (SBC-1), a phosphatic nodule from the Hushpuckney shale of the Swope cyclothem, and a pure apatite reference powder. An extraction modified from Galindo et al. (2007) was used to represent a more standard sequential extraction as it is based on the popular method of Tessier et al. (1979). The extracts were analyzed for uranium concentrations using ICP-MS. The residues that were obtained after each extraction step were also analyzed using XRD and compared qualitatively to gauge the effect of each reagent on relevant minerals.

Two modifications were made to the original Galindo et al. (2007) procedure. First, the initial extraction/soak using D.I. water was removed since preliminary tests showed that the

release of U was negligible (<0.06 ppm for several tested shales, <1% of the total recovered amount). Second, the final total bulk digest (ashing and peroxide fusion) was replaced with a hotplate aqua regia digest due to equipment limitations (the advantages and disadvantages of this replacement are described in more detail in Section 5.1). The final procedure is shown in Table 2, with methodological details described in Appendix D. In addition to the sequential extraction, a separate 0.1g sample of the reference shale (SBC-1) was ashed and digested in a microwave (Table 2, final step) for comparison.

2.2 MODIFIED SEQUENTIAL EXTRACTION PROCEDURE

In addition to the work described above, a second sequential extraction was performed on samples from the Heebner shale. This extraction was based on the procedure listed in Table 1, but with additional modifications (Table 2).

Table 2: Modified sequential extraction and bulk digest procedure. Steps marked with an asterisk were repeated for a total of three iterations (see Appendix D for more information).

Extraction Step	Target phases/objective	Reagent	Reaction/agitation time and parameters
E1	Exchangeable	9 mL 1M $MgCl_2$	24hrs at 25°C
E2	Carbonates	12 mL 1M CH_3COONa + 1M CH_3COOH	24hrs at 25°C
E3	Apatite	12 mL 5% nitric	0.5hrs at 25°C
*E4.1	Humic acids/pyrite	9 mL H_2O_2 + 5 mL 0.02M HNO_3	2hrs at 85°C
*E4.2	Humic acids/pyrite	5 mL H_2O_2 + 3 mL 0.02M HNO_3	3hrs at 85°C
E4.3	Prevention of re-adsorption of analyte	12mL 3.2M CH_3COONa in 20% HNO_3	0.5hrs at 25°C
E5	Partial residual digest	15mL aqua regia	12hrs at 90°C
Separate bulk digest (0.1g of material)	All target materials of extractions E1-E5 + kerogen	Aqua regia (microwave-assisted digestion)	Ashing: 550°C for 12 hours Microwave: 5mL aqua regia, 300W @ 100°C, 15 minutes

There are several differences between the procedures in Table 1 and Table 2. The "F3" step was removed since there are likely no Fe/Mn oxides in the LPMS shales given the reducing character of their deposition. This is supported by the work of Desborough et al. (1991), which found that no Fe or Mn oxides were detectable in outcrop samples of other cyclothem shales. The F3 step was instead replaced by a 5% HNO_3 extraction for 0.5hrs to target apatite minerals. The H_2O_2/HNO_3 extractions were repeated multiple times until effervescence was diminished. The reagent volumes were adjusted proportionally to 1g starting sample sizes to conserve material, rather than the 3g sizes used in the procedure in Table 1 and the original Galindo et al. (2007) procedure.

Separate 0.1g samples of the same powders were ashed and then partially digested in a microwave to get bulk values. The resulting supernatants were analyzed for U and other trace metal data and compared with the recovery of the sequential extraction. Both the microwave-assisted bulk digest and the sequential extraction procedures are tabulated in Table 2, and details of the methodology are described in Appendix D.

The Heebner shale samples were collected from three outcrops in 5cm intervals. The outcrop locations create a transect that runs roughly NE-SW (paleo-direction) along the midcontinent shelf of the LPMS (Figure 1). Pre-collected nitrogen isotope and %C data (Turner 2014) were available for these samples and were used to sub-select samples that cover the extent of the nitrogen isotope excursions that are present at each outcrop. The extracts were analyzed using ICP-MS for uranium concentrations.

2.3 ICP-MS METHODS

The extracts obtained through the sequential extractions in Tables 1 and 2 were analyzed on a Thermo iCap Qc ICP-MS for uranium concentrations using a standard addition method, which compensates for matrix effects (Harris 2010). For this method, three or more tubes that contain equal amounts of the diluted solution are prepared. A known amount of a standard for the analyte of interest is added to one of the tubes in order to increase the instrument response (intensity, in counts per second) by 1.5-3 times the reading of the unspiked solution. Another tube is spiked so that its response is 2-3x the reading of the first spiked tube. This process is continued for the desired amount of repetitions (two spiked solutions were used in this study). Dilute nitric acid is then added to the tubes so that the end solution masses are equal. A plot of concentration vs intensity yields a linear trend that can be extrapolated to a point on the negative x-axis. When adjusted for dilution, this represents the concentration of the unspiked solution.

The extracts from the microwave-assisted digestion of the separate 0.1g Heebner samples were analyzed for U and other trace metals (Appendix A) using an external calibration technique (modified from EPA method 200.8). In this method, precisely weighed aliquots of each stock solution were dried down in Teflon containers and brought back up in 2% nitric acid. These solutions were then diluted to an appropriate level and analyzed. The values were calibrated to multi-element standards (Inorganic Ventures 2008-Cal1, 2008-Cal2). Aliquots of

these standards were mixed together and multiple (3) dilutions were prepared in order to create a calibration curve. A second multi-element standard was prepared similarly and used as a quality check (IV-ICP-MS-71A). Instrument drift and suppression effects were corrected using an internal standard (IV-ICP-MS-71D). The external calibration method requires less preparation but has lower accuracy, particularly when comparing samples with variable amounts of dissolved solids. To minimize the degradation of accuracy, the estimated total dissolved solid content was kept below 0.2% w/v. The same external calibration method was also used for uranium analysis of the separate microwave-assisted digestion of the Heebner samples.

2.4 XRD Methods

XRD analysis was used in two different ways. First, 0.1g of residue from each step of the "standard" sequential extraction (Table 1) that was performed on the LPMS-analogous Permian shale, reference shale SBC-1, and the phosphatic nodule were collected and analyzed using bulk powder XRD to qualitatively compare the changes in composition over the course of the extractions. This data is presented as stacked diffractograms for relevant minerals in Section 4.4. The Heebner samples were pressed into 0.5g pellets and analyzed for bulk mineralogical data. All analysis was done in Jade v6.1.

The sample powders were micronized prior to the extractions or bulk analysis to improve XRD results by eliminating particle size effects. Deionized water was chosen as the micronization medium rather than ethanol to prevent any loss of soluble organics. The loss of U from these materials in water was generally low; earlier tests indicated that after an overnight soak the water contained 0.06 ppm for the Permian shale, 0.03 ppm for SBC-1, 0.45 ppm for the pure apatite, and 0.07 ppm for the phosphatic nodule (according to ICP-MS analysis). These values are considered negligible in comparison to the total U recovered from these materials by the sequential extractions (11.96, 2.19, 101.47, and 168.98 ppm, respectively). For the Heebner samples, chemically untreated micronized powders were pressed into 0.5g pellets and analyzed for bulk mineralogy. Analysis was performed in Jade 6.1 and the data were processed for semi-quantitative mineral weight percentages using a method modified from Cook et al. (1975), which is described below.

Interference-free diagnostic peaks for each detected mineral were chosen, and the peak heights were weighted using intensity factors from Cook et al. (1975) which were determined from 50:50 mixtures of mineral standards with pure quartz. An estimated relative weight percentage is given by the weighted peak height divided by the integrated weighted peak heights for all detectable minerals. Given the inaccuracy inherent to quantifying clay minerals without the preparation of <2 μM clay separates, a "composite" peak was chosen that represents the combined influence of all clays (d-spacing 4.33 to 4.55, intensity factor = 20) to estimate clay content. This approach will not accurately estimate the weight percentage of clay minerals, and by extension the estimated weight percentages of the other detected minerals are made inaccurate.

However, this method allows for the mineral abundances to be compared qualitatively. An estimate of error is not available with the current data. A possible way to calculate error for this method would be to prepare and analyze samples that contain known but variable "spikes" of standard material that are otherwise replicates. The degree to which qualitative robustness is maintained would provide an estimate of the error.

Due to interference between the strongest diagnostic peak of pyrite at ~1.62 (d-spacing) and the second strongest peak of fluorapatite, a weaker pyrite peak was used. As a result, samples with low pyrite content are reported as "0", although in reality this is likely a small nonzero number. The intensity factor for the chosen quartz peak is relative to the intensity factor reported by Cook et al. (1975), and was determined experimentally using quartz standards. The Cook et al. (1975) recommendation for quartz was not used to prevent interference with illite. The diagnostic peaks and intensity factors that were used for each of the detected mineral are shown below in Table 3.

Table 3: Diagnostic peaks and intensity factors used in the semi-quantitative analysis of mineral composition for the Heebner shale samples, from Cook et al. (1975). The alternative quartz intensity factor was determined relative to the value reported by Cook et al. (1975).

MINERAL	D-SPACING RANGE	INTENSITY FACTOR
Apatite	2.78 - 2.81	3.10
Calcite	3.01 - 3.04	1.65
Quartz	4.20-4.30	5.08
Pyrite	1.62 - 1.63	2.30
Dolomite	2.87 - 2.90	1.53
Plagioclase	3.16 - 3.21	2.80
"Total Clay"	4.33 - 4.55	20.00

2.5 $\delta^{15}N$ EXCURSIONS, %C (PRE-COLLECTED DATA)

Nitrogen isotope data ($\delta^{15}N$) and %C were available from Turner et al. (2014), with analysis performed at The University of Cincinnati Department of Geology. The total %C values were obtained through isotope ratio mass spectrometry using non-acidified bulk samples. Nitrogen isotopes are presented here as $\delta^{15}N$, which is defined as:

$$\delta^{15}N = (((^{15}N/^{14}N)_{sample} / (^{15}N/^{14}N)_{standard}) - 1) \times 1000$$

Atmospheric nitrogen was used as the standard. Samples were weighed out for analysis into tin capsules and analyzed on a Thermo Delta V IRMS coupled to a Costech 4010 EA.

CHAPTER 3: RESULTS

3.1 URANIUM PARTITIONING OF RELEVANT MATERIALS ACCORDING TO A "STANDARD" SEQUENTIAL EXTRACTION

All data for these tests are tabulated in Table 4 and shown as bar graphs in Figure 5. For the "standard" sequential extraction (Table 1) performed on the Permian and SBC-1 reference shale, the majority of the extracted U was in the organic and pyrite-associated fractions released concomitantly in extraction steps F4.1-F4.3. The second-most enriched extracts for both samples were from the residual (F5) aqua regia digest.

Table 4: Uranium concentrations of the extracts from the "standard" sequential extraction performed on black shale from a Permian cyclothem, a phosphatic nodule, a UGSS reference shale (SBC-1), and a pure apatite powder. The discrepancy between the U recovery for the extractions and the listed value for SBC-1 is discussed in Section 5.1.

Extraction	SBC-1	Permian Shale	Phosphatic Nodule	Pure Apatite
F1	0.044	0.36	1.66	0.57
F2	0.2	1.04	11.58	11.25
F3	0.1	0.17	19.61	12.26
F4.1/F4.2	0.52	5.87	30.93	9.46
F4.3	0.77	2.61	105.14	67.93
F5	0.56	1.91	0.06	0
Total F1-F5	2.19	11.96	168.98	101.47
Certified Value	5.76	n/a	n/a	n/a
Microwave Digestion	2.63	n/d	n/d	n/d

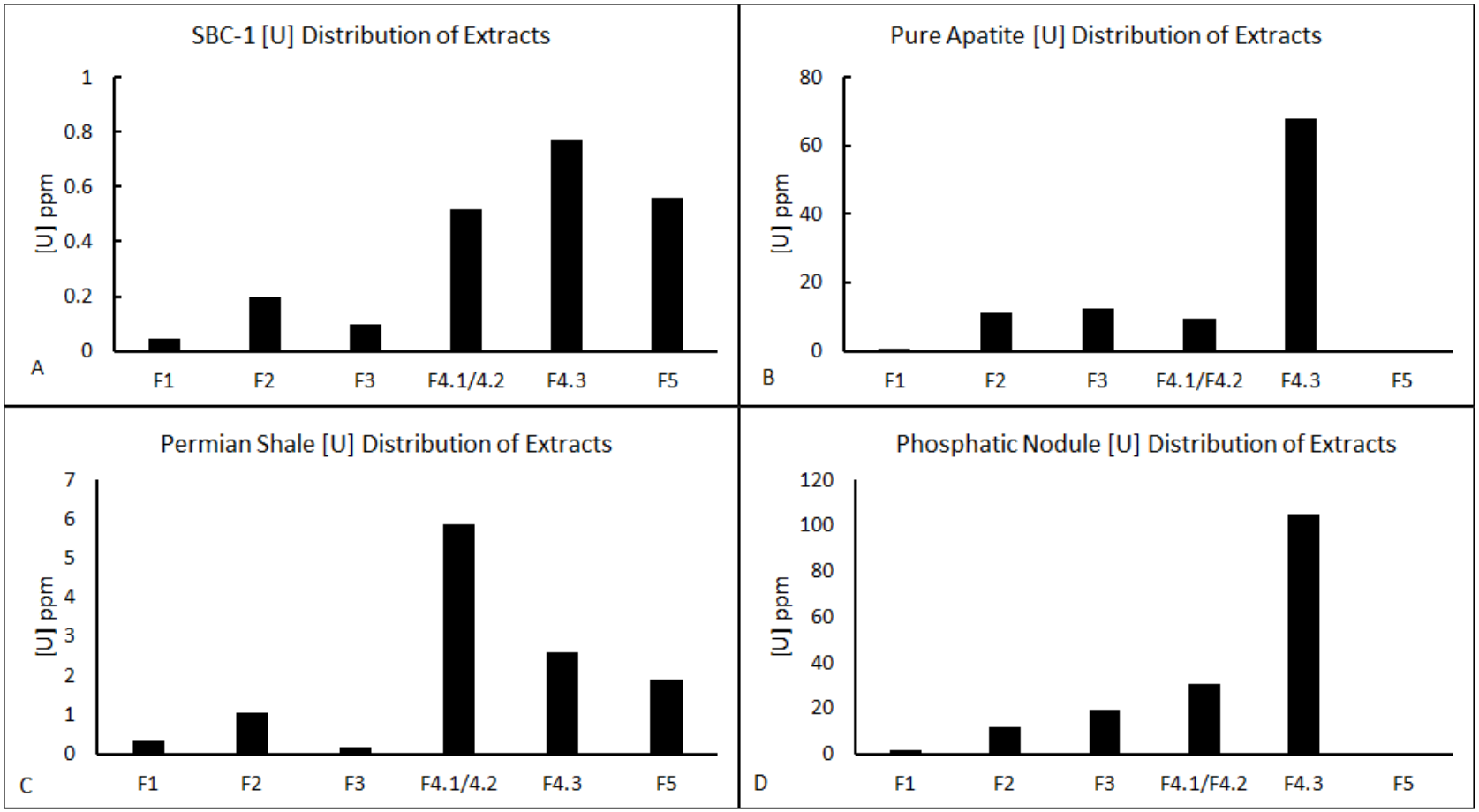

Figure 5: Uranium partitioning of select materials according to a "standard" sequential extraction (Table 1). The tested materials are a USGS reference shale (SBC-1) (A), a pure apatite (B), an LPMS-analogous Permian cyclothem shale (C), and a phosphatic nodule from the Hushpuckney Shale (D). Targets of extraction steps: F1 – exchangeable metals, F2 – carbonates, F3 – Fe/Mn oxides, F4.1-F4.3 – organics/pyrite, F5 – aqua regia soluble

3.2 $\delta^{15}N$ EXCURSIONS, %C (PRE-COLLECTED DATA)

$\delta^{15}N$ excursions are apparent in all three outcrops. The Sedan outcrop exhibits smooth rising and falling trends, while the Clinton outcrop has a forked peak. The I229 outcrop shows only the falling limb of the excursion and part of the peak; this may be the result of sampling error or possibly the initiation of the excursion during the deposition of the underlying limestone. The excursions and %C (inclusive of inorganic C) values are shown along with the sequential extraction and XRD data for the Heebner samples in the following results sections (Figures 6-8, 12-14).

It is convenient to divide the samples into zones according to the nitrogen excursions following the method of Herrmann et al. (2012, 2015). Zone I corresponds to the rising limb of the excursion up to the peak. Zone II (middle black shale) encompasses the falling limb. Together, Zones I and II encompass the lower fissile portion of the black shale. Zone III (upper black shale) comprises the less fissile upper halve of the black shale unit and terminates at the overlying gray shale. The boundary between Zone II and Zone III corresponds to a lithological transition (fissile shale to blocky) and may also record the maximum flooding surface (Algeo et al. 2004, Algeo et al. 2008).

3.3 URANIUM DISTRIBUTION IN THE HEEBNER SHALE

The uranium distribution within the Heebner shale is variable with respect to both time and space. The [U] of the extracts for each outcrop is plotted moving upsection along with the nitrogen excursions and %C in Figures 6-8. The total cumulative error for the sequential extraction and quantification of the extracts (as estimated from the difference between the total recovery of U of the main run and a replicate analysis) is +/- 0.06 ppm. The estimated cumulative error for the external calibration method is estimated similarly to be +/- 0.34 ppm. The individual errors for each extraction step as determined from the replicate analysis are listed in the figure captions where the data are presented (Figures 6-8). For the vast majority of the samples the E1 extraction yielded a low amount of U (average all samples: 0.18 ppm, SD 0.27). The E1 values are reported in Appendix A (Table 10) but are not included in the following discussions.

The Sedan outcrop was notably less enriched overall, with values ranging from 1.41 to 5.07 ppm for the sequential extraction and 2.52 – 8.35 ppm for the microwave-assisted digestion of the same samples. The Clinton and I229 outcrops were more enriched, but with a larger degree of variability that was primarily driven by high U concentrations in the E3 extracts for some samples. Enrichment in the E3 extracts peak in all three outcrops at the termination of the nitrogen excursion or on the falling limb, but the peak is broader and more pronounced in the Clinton outcrop. When the sampled intervals are considered as a whole, the microwave-assisted digests of the Clinton and I229 outcrops contain averages that are in line with previously published estimates (~30ppm, Doveton & Merriam 2004, Watney 1979, Coveney and Glascock 1989)

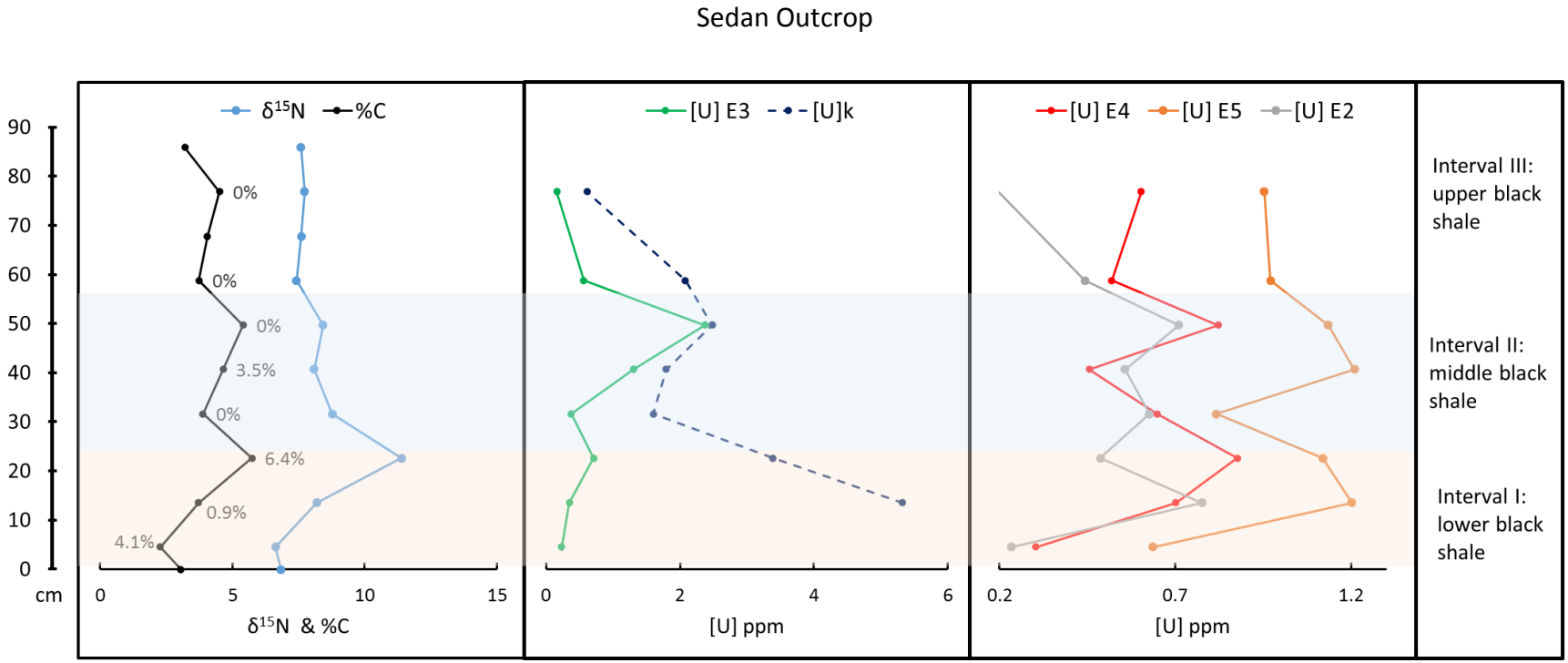

Figure 6: U concentrations of the extracts from the modified sequential extraction (Table 2) for the Sedan outcrop sample set, plotted with the recorded nitrogen excursion and %C (with wt. % carbonate listed when available). The zones are divided based on the nitrogen excursions (Section 4.1). The [U]k value (dashed line) is the difference between the U recovery from a separate ashing and microwave assisted digestion and the recovery from the modified sequential extraction (Table 2). Targets of extraction steps: E2 = carbonates, E3 = apatite, E4 = Organics + Pyrite, E5 = residual material

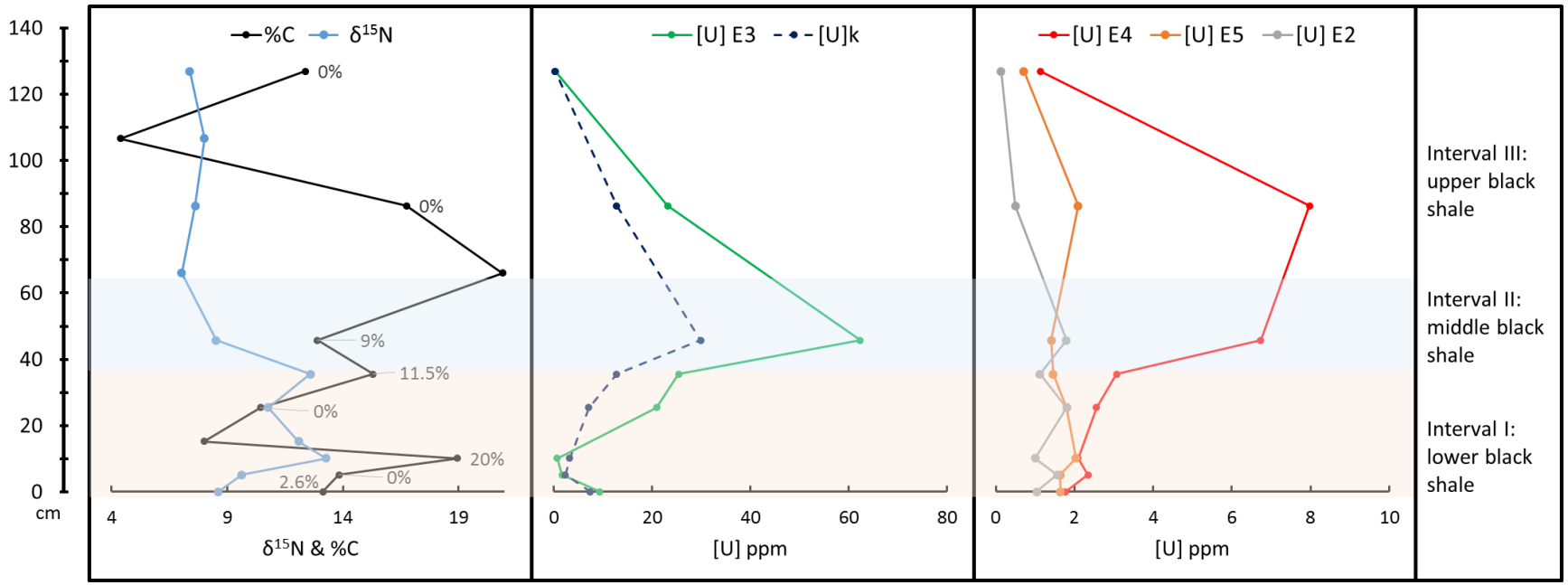

Figure 7: U concentrations of the extracts from the modified sequential extraction (Table 2) for the Clinton outcrop sample set, plotted with the recorded nitrogen excursion and %C (with wt. % carbonate listed when available). The zones are divided based on the nitrogen excursions (Section 4.1). The [U]k value (dashed line) is the difference between the U recovery from a separate ashing and microwave assisted digestion and the recovery from the modified sequential extraction (Table 2). Targets of extraction steps: E2 = carbonates, E3 = apatite, E4 = Organics + Pyrite, E5 = residual material

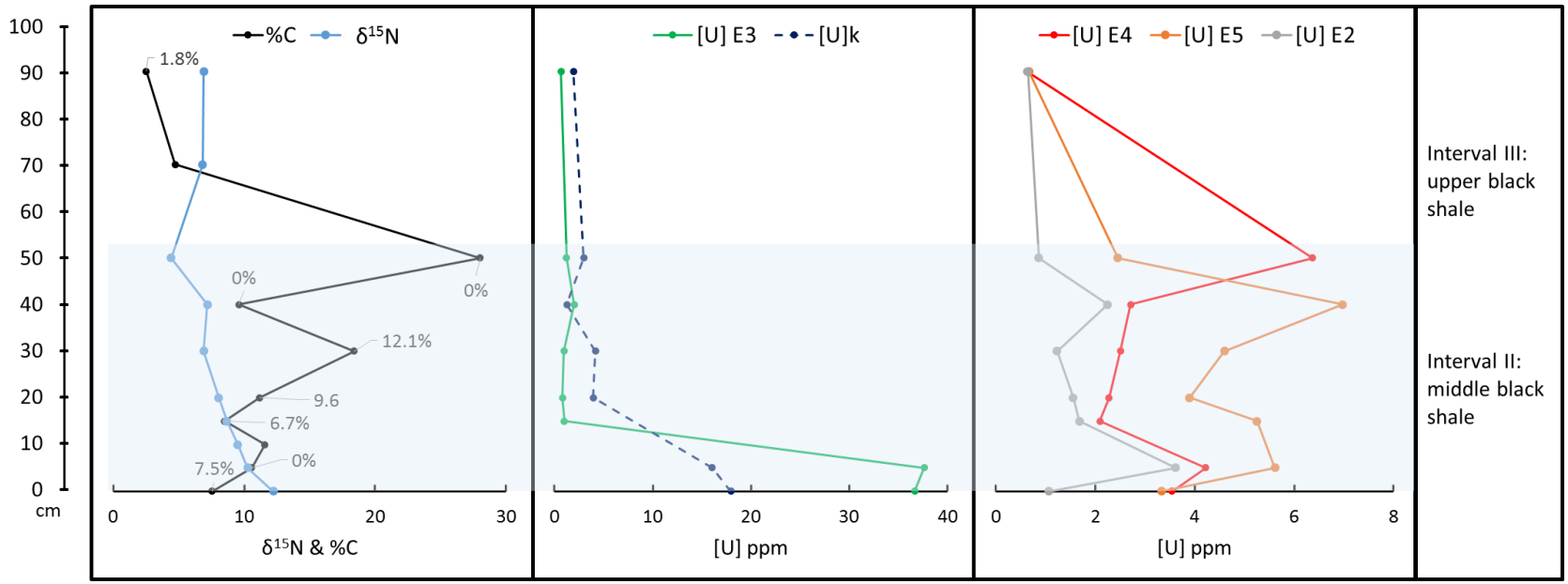

Figure 8: U concentrations of the extracts from the modified sequential extraction (Table 2) for the I229 outcrop sample set, plotted with the recorded nitrogen excursion and %C (with wt. % carbonate listed when available). The zones are divided based on the nitrogen excursions (Section 4.1). The [U]k value (dashed line) is the difference between the U recovery from a separate ashing and microwave assisted digestion and the recovery from the modified sequential extraction (Table 2). Targets of extraction steps: E2 = carbonates, E3 = apatite, E4 = Organics + Pyrite, E5 = residual material

3.4 RESPONSE OF MINERALS TO EXTRACTION REAGENTS

Since the effects of the extractions on apatite are of particular importance for the study of uranium, the mineral composition of the residues obtained after each extraction step performed on the phosphatic nodule was calculated using the method described in Section 3.4 to quantify any partial digestion (Table 5). The minor presence of clay in the nodule were ignored and the residues were treated as a two component mixture (quartz and fluorapatite). A decrease in the abundance of fluorapatite before it is completely digested is apparent in steps F3 and F4.1/F4.2 (relative to quartz).

Table 5: Composition of a phosphatic nodule after each step of a "standard" sequential extraction. Minor contributions from clay was ignored in the calculations.

Residue	% Fluorapatite	% Quartz
(Control)	67	33
F1	66	34
F2	67	33
F3	62	37
F4.1 / F4.2	58	42
F4.3	0	100%

The Permian shale contains quartz, illite, kaolinite, Fe-rich chlorite, plagioclase, pyrite, fluorapatite, and calcite (Appendix B: Figures 19, 20, and 23). All listed minerals for SBC-1 were detected and are shown in Figures 9-11 (quartz, muscovite, rutile, anatase, pyrite, calcite, siderite, kaolinite, and chlorite). The phosphatic nodule contains mainly quartz and fluorapatite with minor amounts of clay (Figure 10, Figures 21 and 22 in Appendix B). The effect of each reagent of the "standard" sequential extraction (Table 1) on the detected minerals in the Permian cyclothem shale, reference shale SBC-1, and the phosphatic nodule are shown in Figures 9-11. Between these three materials, all minerals that are in the Heebner samples are represented except dolomite. Since the "standard" sequential extraction (Table 1) uses the same reagents as the procedure used on the Heebner (Table 2) with the exception of the third steps ("F3" vs "E3"), the effect of the modified extraction procedure on the mineral constituents of the Heebner can be inferred.

Calcite and pyrite were dissolved in the intended extractions (F2 step and F4.1/F4.2 respectively, Figures 9 and 10). Siderite was mostly unaffected by the F1-F3 extractions, but was partially digested in F4.1/F4.2 and completely digested in step F4.3. Illite and kaolinite are not noticeably affected by any of the extractions (Figure 10). The only susceptible clay was chlorite, which was quantitatively removed in F5 (Figure 9). Fluorapatite is only noticeably affected by the F5.3 step, where it is completely digested (Figure 10). Rutile is unaffected by all steps (Figure 9). Due to interference, anatase is only detectable when chlorite is digested in the F5 extraction, and appears as a peak at ~25.4 (2θ). Like rutile, anatase is also unaffected by the reagents as would be expected given the resilience of titanium oxides (Xu et al. 2012), (Figure 11).

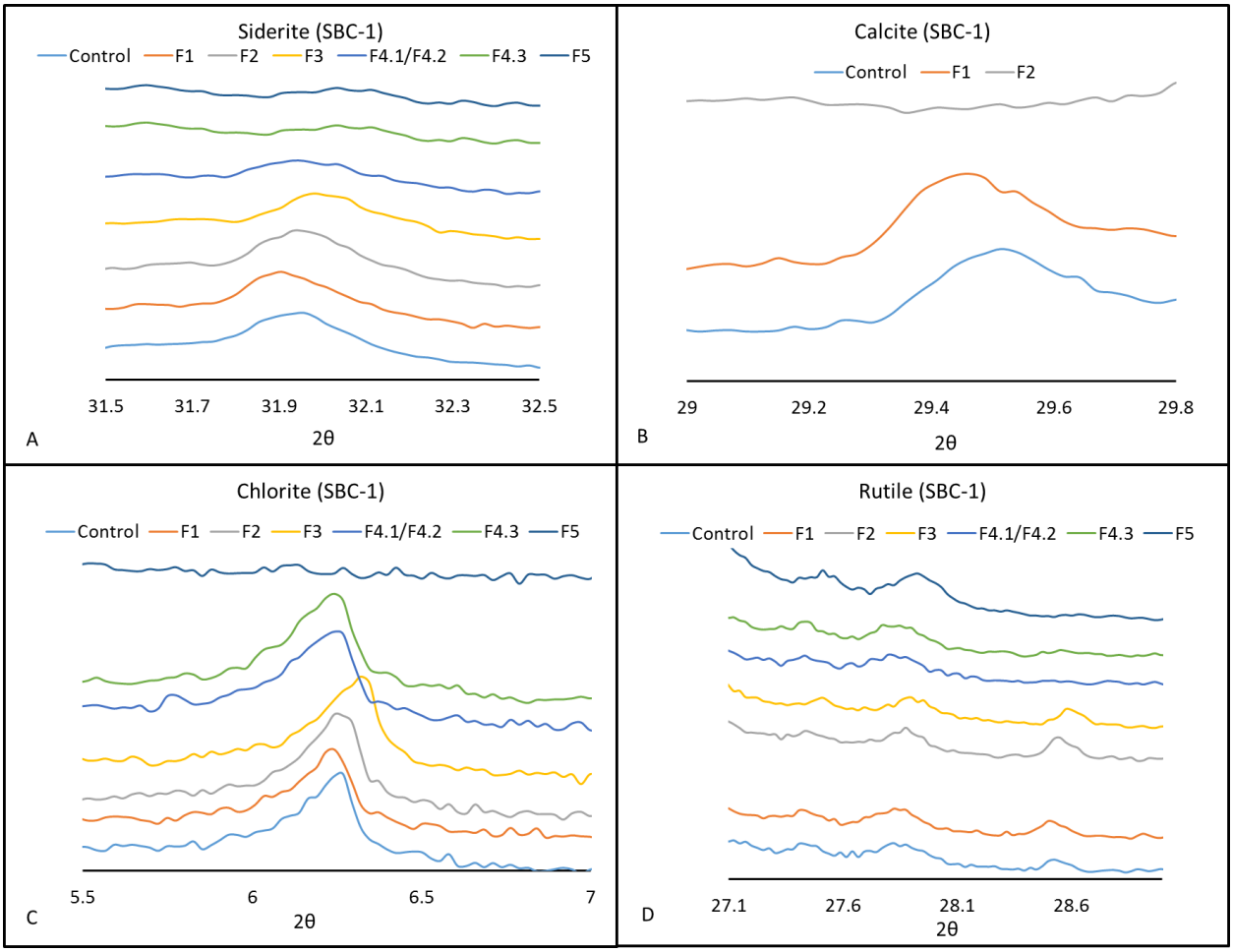

Figure 9: Response of siderite, calcite, chlorite, and rutile to a "standard" sequential extraction (Table 1). Siderite (A) is relatively unaffected by steps F1-F3, whereas it's partially digested in steps 4.1/4.2 and entirely removed in step 4.3. Calcite (B) is removed in its intended extraction step (F2). Chlorite (C) is unaffected by steps F1-F4.3, but is completely digested in step F5. Rutile (D) (diagnostic peak at ~27.4 2θ) is unaffected by all reagents. Intended targets of extraction steps: F1 = exchangeable, F2 = carbonates, F3 = Fe/Mn-oxides, F4.1-F4.3 = organics and pyrite, F5 = residual (aqua regia soluble).

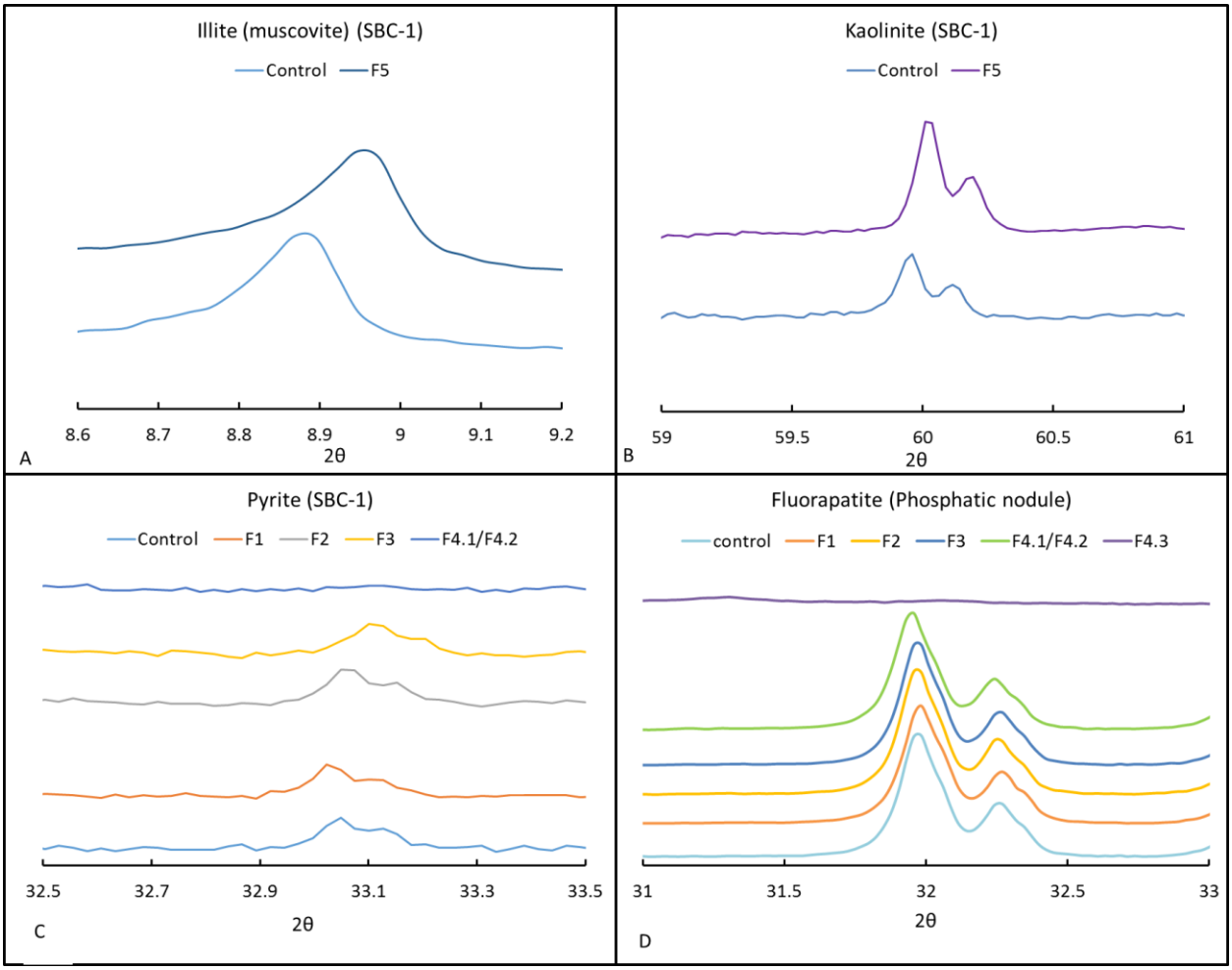

Figure 10: Response of illite, kaolinite, pyrite, and fluorapatite to a “standard” sequential extraction (Table 1). Illite (A) and kaolinite (B) are unaffected by all reagents. Pyrite (C) is removed in the F4.1/F4.2 steps as intended. Fluorapatite (D) appears to be relatively unaffected by steps F1-F4.2, but is completely digested in step F4.3. The release of apatite in this step inflates the trace element content assigned to organics and pyrite according to a standard sequential extraction scheme. Intended targets of extraction steps: F1 = exchangeable, F2 = carbonates, F3 = Fe/Mn-oxides, F4.1-F4.3 = organics and pyrite, F5 = residual (aqua regia soluble)

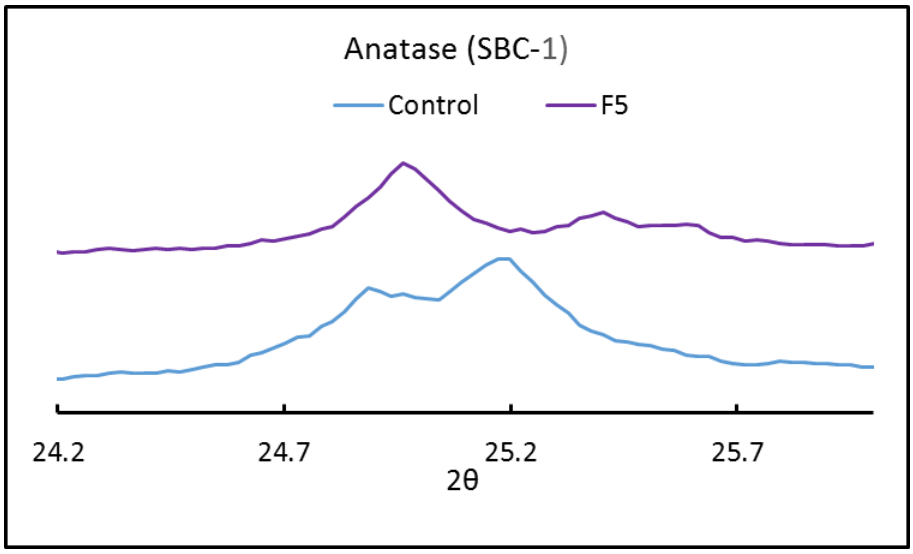

Figure 11*:* Response of anatase to a "standard" sequential extraction (Table 1). The presence of this mineral is not detectable before step F5 (aqua regia) due to interference with chlorite, which is removed in that step. The peak at ~24.9 (2θ*)* corresponds to kaolinite, which is unaffected by the extraction. Anatase is identified by the peak around 25.4 (2θ).

3.5 XRD CHARACTERIZATION OF THE HEEBNER SHALE

All analyzed samples of the Heebner shale contain quartz, illite, kaolinite, Fe-rich chlorite, and plagioclase. Other detected minerals present in some samples include fluorapatite, pyrite, calcite, and dolomite. The relative mineral abundances are reported as estimated weight percentages and plotted with the nitrogen isotope excursions and %C for each outcrop moving upsection in Figures 12-14. With the current data a valid estimate of error is not possible (see Section 2.4 for more information).

Peaks in apatite content at each outcrop occur in Interval II of the nitrogen excursions. This peak is most prominent for the Clinton samples and least for the Sedan samples. Pyrite and carbonate minerals (dolomite and calcite combined) covariate positively in the Clinton and I229 outcrops, but not in the Sedan outcrop. The Clinton outcrop generally contains more authigenic minerals (apatite and carbonate) and more variable accumulation of pyrite.

Although TOC is not available, the %C values and the estimated carbonate mineral content shown in Figures 12-14 can be used to infer where the %C are influenced by inorganic C. A possible low carbonate %C peak is apparent in the Sedan and I229 outcrops and possibly the Clinton outcrop around the termination of Interval II.

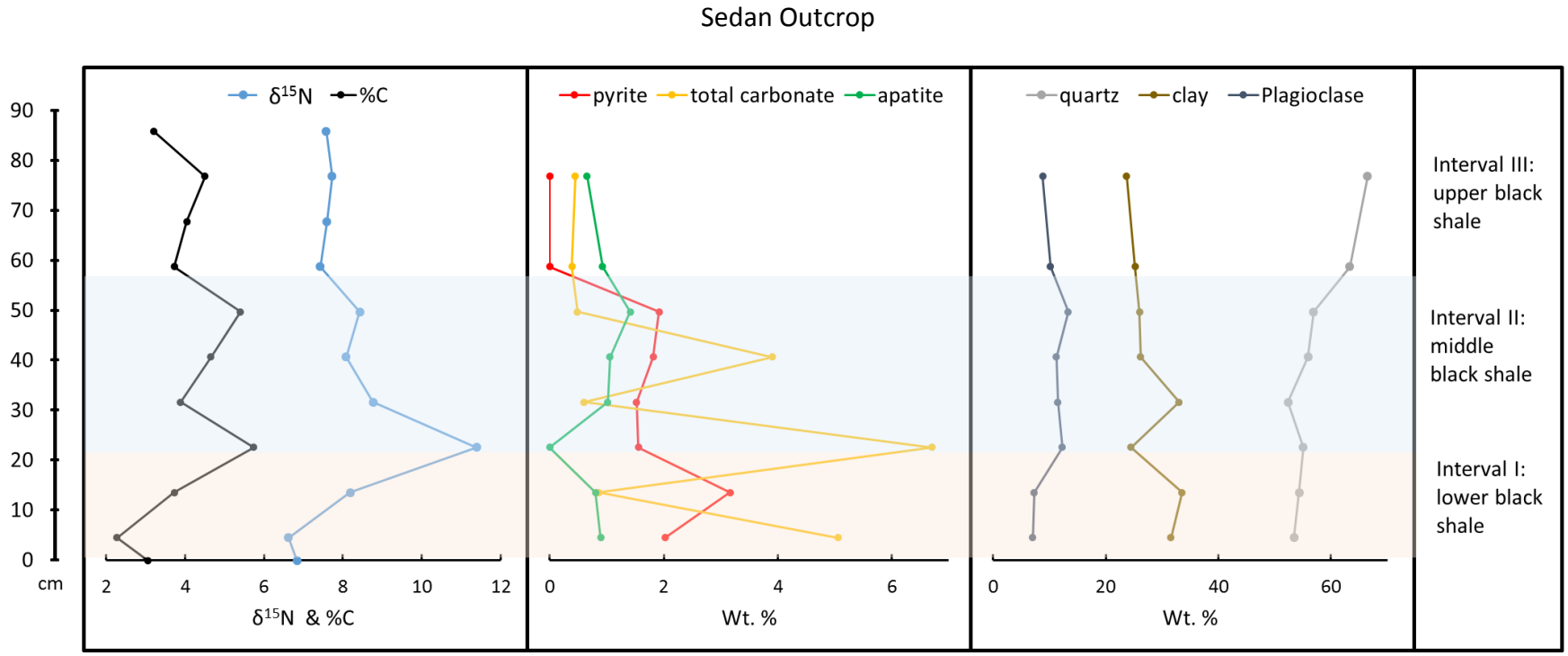

Figure 12: Mineralogical changes of the Sedan outcrop samples of the Heebner shale moving upsection, with the recorded nitrogen excursion and %C. Intervals I, II, and III correspond to sections of the nitrogen excursion as outlined in Herrmann et al. (2008, 2015). See section 2.5 for information regarding estimation of error.

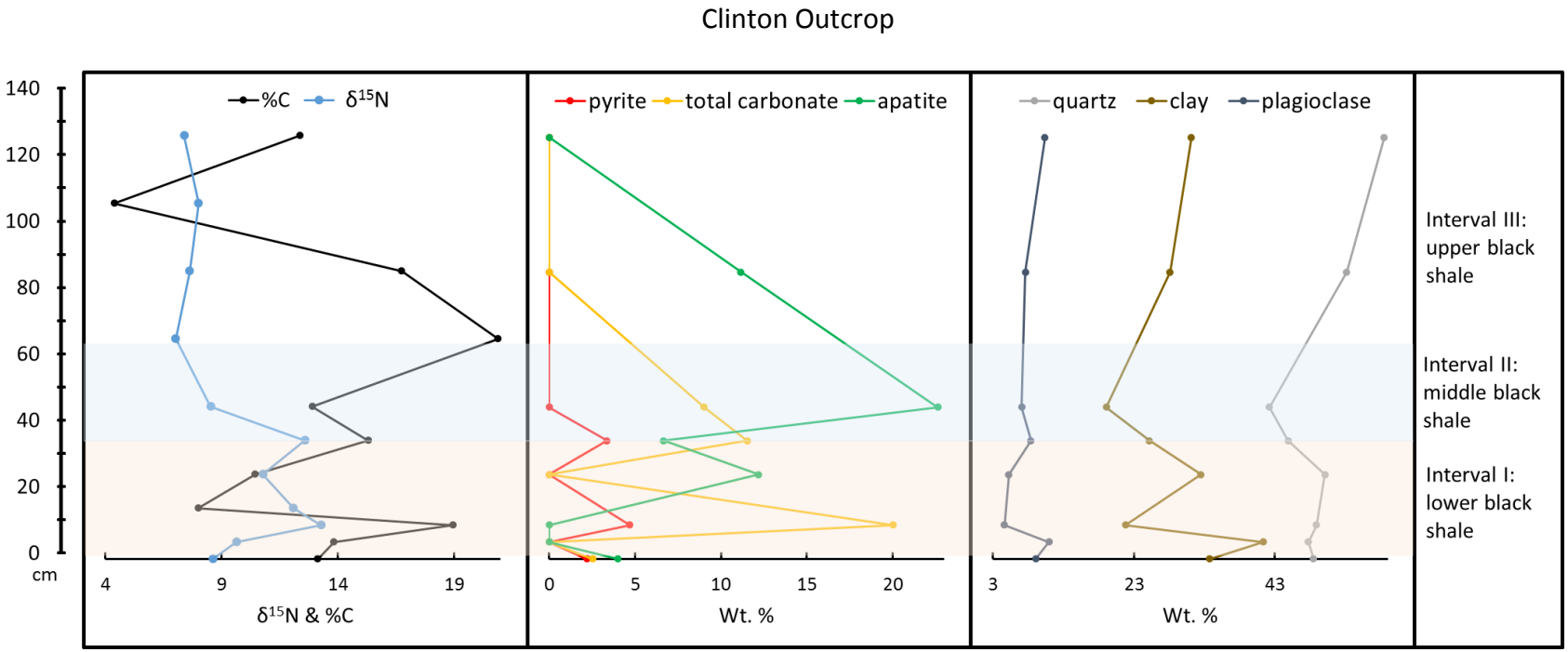

Figure 13: Mineralogical changes of the Clinton outcrop samples of the Heebner shale moving upsection, with the recorded nitrogen excursion and %C. Intervals I, II, and III correspond to sections of the nitrogen excursion as outlined in Herrmann et al. (2008, 2015). See section 2.5 for information regarding estimation of error.

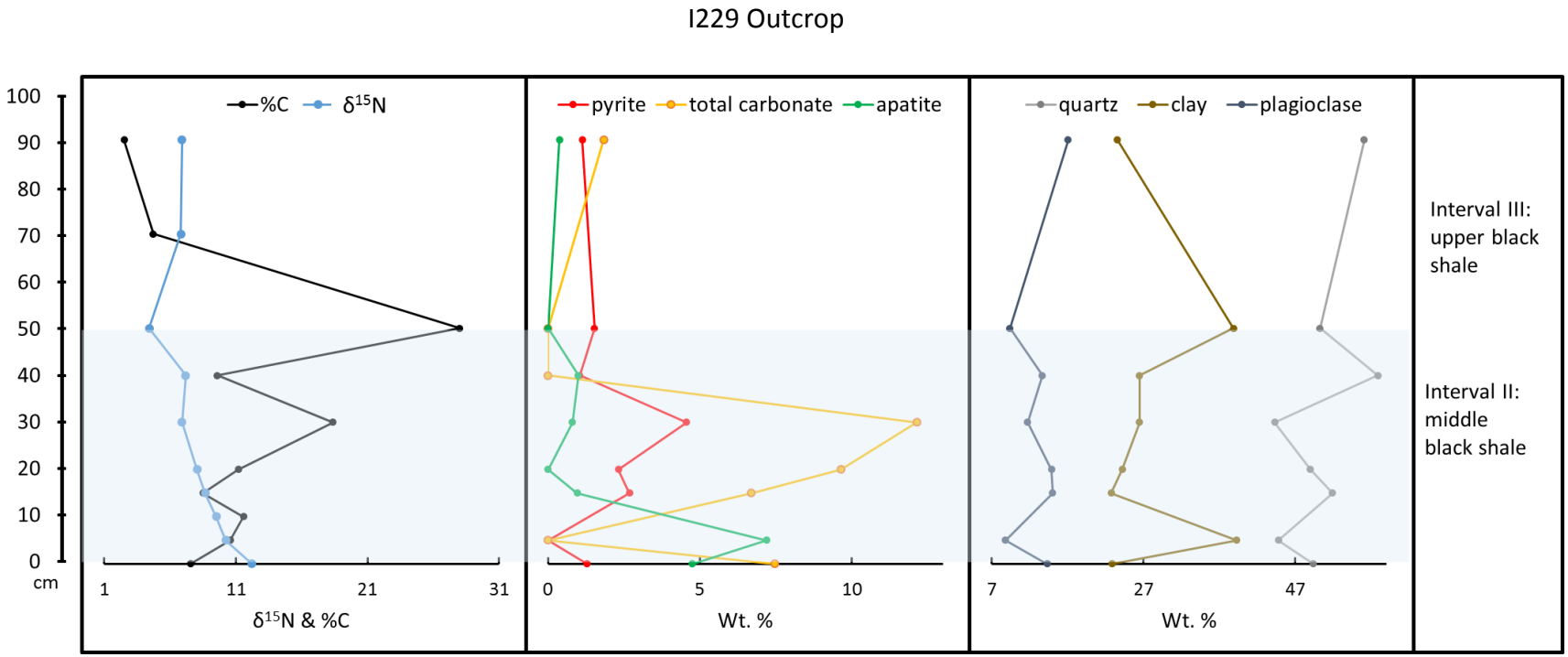

Figure 14: Mineralogical changes of the I229 outcrop samples of the Heebner shale moving upsection, with the recorded nitrogen excursion and %C. Intervals I, II, and III correspond to sections of the nitrogen excursion as outlined in Herrmann et al. (2008, 2015). See section 2.4 for information regarding estimation of error.

CHAPTER 4: DISCUSSION

4.1 EFFICACY OF SEQUENTIAL EXTRACTIONS

4.1.1 E1/F1 Extraction

The low yield of the F1/E1 extractions suggest that exchangeable uranium is not an important fraction in any of the materials. This fraction includes weakly surface-bound metals (Zerbe et al. 1999) that are available for interaction with common ions (e.g. Mg, Ca, K, Na) that are often present in pore fluids or sediment. Metals in this fraction can't easily be tied to a specific host, and are associated with any particle that contains them in a diffuse ion association or an outer sphere complex (i.e. a hydration shell, McLean & Bledsoe 1992). While the low U concentration and the lack of specificity of the F1/E1 extracts would imply that this extraction is unnecessary for uranium analysis of black shale, it may have a use in preconditioning the sample to prevent contamination of the following extracts with the small but nonspecific exchangeable contribution.

4.1.2 F2/E2 Extraction

The F2/E2 extractions accomplished their primary goal of dissolving calcium carbonates. Figure 9 shows that calcite is removed quantitatively. No XRD data are available to show the dissolution of dolomite, but it has been shown to be effective when the amount of dolomite in the sample is not excessive (Tessier et al. 1979), and presumably the long reaction time (24hrs) is sufficient for complete dissolution.

Two potential pitfalls with the F2/E2 carbonate extractions are apparent. The first is the inability to digest siderite ($FeCO_3$), which is only extracted in the F4 steps (Figure 9). Although siderite was not detected in any of the Heebner samples, it is present in other LPMS shales (Desborough et al. 1991). A laboratory absorption/desorption study by Ithurbide et al. (2010) has shown that siderite can adsorb U on its surface and then precipitate it as U^{IV} from low-carbonate uranyl solutions. This implies the precipitation of a reduced uranium mineral (i.e. uraninite, UO_2) which has some solubility in buffered acetic acid solutions (Quejido et al. 2005). A second potential problem with the F2/E2 carbonate extraction is the premature digestion of apatite. While the XRD tests (Figure 10, Table 5) suggest that fluorapatite is minimally affected by the reagents preceding step F4.3, the release of U in the F3 and F4.1/F4.2 steps for both the phosphatic nodule and pure apatite suggest that there was a degree of dissolution (Table 4, Figure 5). The type of fluorapatite present in the phosphatic material of the LPMS shales has previously been identified as francolite, or authigenic carbonate fluorapatite (Runnels 1953, Kidder 1985, Hoffman et al. 1998), which is represented by the general formula $Ca_{10-a-b}Na_aMg_b(PO_4)_{6-x}(CO_3)_{x-y-z}(CO_3{\cdot}F)_y(SO_4)_zF_2$ (Tribovillard et al. 2006).

Francolite has been described as being fully soluble in buffered acetic acid solutions (Ruttenberg 1992), or alternatively as mostly insoluble (Vaimakis 1998). Extensive carbonate substitution into the fluorapatite crystal structure increases its susceptibility to acid (Nathan

1984), but decarbonization (and greater resistance to acid) tends to occur with age and exposure to weathering (McClellan & Saavedra 1986). In this regard, different samples of francolite will respond to the E2/F2 reagent variably, with recent material likely to be more susceptible to dissolution. From the XRD and U concentration data (Table 4, Table 5), it appears that the nodule fluorapatite was only minimally soluble in a pH=4.75 buffered acetic acid solution, but released a disproportionate amount of U. This effect can be seen in Figures 6-8, where the larger peaks of $[U]_{E3}$ coincide with peaks of $[U]_{E2}$ despite a lack of carbonate minerals. Despite this potential for selectivity issues, the $[U]_{E2}$ extraction overall appears to be reflective of the carbonate contribution in the Heebner, particularly with regards to dolomite, as implied by the positive correlation between dolomite wt. % and $[U]_{E2}$ (Figure 15,B).

4.1.3 F3/E3 Extraction

The third steps for each of the two extraction procedures were different. In F3 the extraction targeted Fe-Mn oxides (Permian shale, SBC-1, phosphatic nodule), and the E3 extraction replaced this reagent with 5% HNO3 to target apatite (Heeber samples). The assumption that the Heebner does not contain Fe/Mn oxides based on its reducing character and the XRD study of other shales by Desborough et al. (1991) proved to be valid since these minerals were not detected through XRD (Section 4.5).

Unless a black shale is suspected of containing Fe/Mn oxides, the F3 step should be replaced, particularly for phosphatic shales due to the partial digestion of fluorapatite in this step and the subsequent release of U and other trace metals. The E3 step that used 5% HNO3 appears to reflect the apatite contribution given the correlation between wt. % apatite and $[U]_{E3}$ (Figure 16). Low apatite samples (<1%) also have low $[U]_{E3}$ values, which suggests no other significant U-carrying material contributed to this fraction.

Since HNO_3 is a strongly oxidizing acid, a valid concern is that reduced minerals such as pyrite or uraninite could be prematurely dissolved. However, a study of the depyritization of coal with HNO_3 at varied concentrations and temperatures found that 5% nitric at room temperature is only able to digest 3% of the total pyrite (Karaca et al. 2003). Uraninite has similarly low dissolution rates without higher temperatures, greater nitric concentration, or the addition of other oxidants (Yauike et al. 1991, Asano et al. 1995, Kataoka et al. 1995, Kim et al. 2000).

Overall, the results indicate that standard sequential extractions that include a Fe/Mn oxide extraction step are not appropriate for phosphatic shales because the contribution from apatite would inflate the apparent contribution from Fe/Mn oxides and organic matter/pyrite. The replacement step with 5% HNO3 appears to be effective for the amount of apatite present in the LPMS shales. An alternative reagent for this step is dilute HCl, which is less oxidizing than HNO_3 and may minimize “contamination” from labile organics and pyrite, although this reagent would digest chlorite.

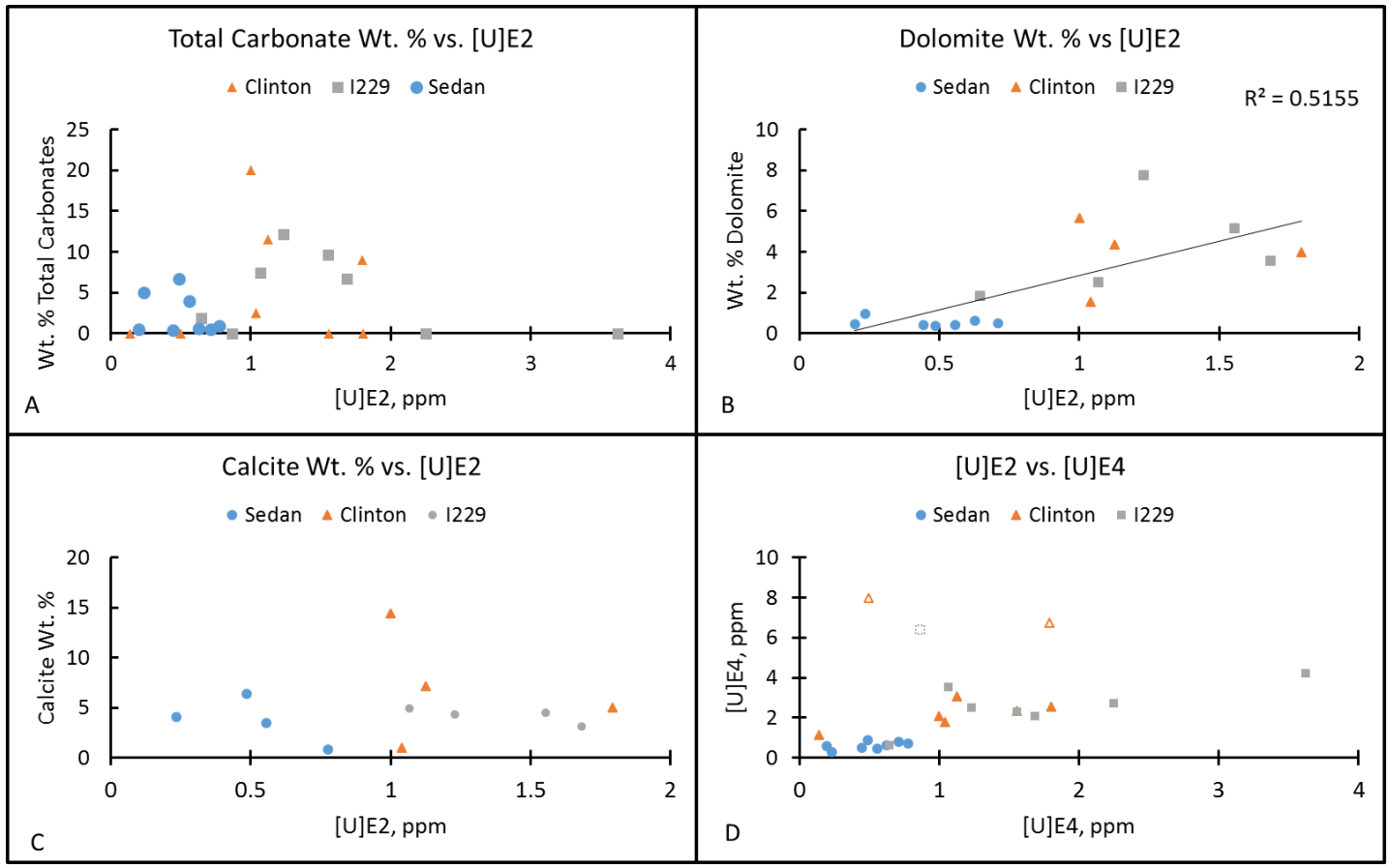

Figure 15: $[U]_{E2}$ vs. $[U]_{E4}$ and $[U]_{E2}$ vs carbonate mineral abundances. In (A), no trends are apparent when the total carbonate abundance (calcite wt. % + dolomite wt. % combined) are compared with $[U]_{E2}$. The correlation between dolomite wt. % and $[U]_{E2}$ (B) suggests that dolomite is more enriched than calcite (C), and is responsible for most of the U released by the E2 extraction. The good correlation between [U]E2 and [U]E4 (D), with the exception of three outlier data points that are associated with the %C peaks in the Clinton and I229 outcrops, suggests that carbonate and organic U enrichment are related. The error as estimated through replicate analysis for both $[U]_{E2}$ and $[U]_{E4}$ is +/- 0.01 ppm. Since no estimate of error is available for the mineral weight percentages (see section 2.4) all error for the trend line calculation in (B) is assumed to reside in the concentration values.

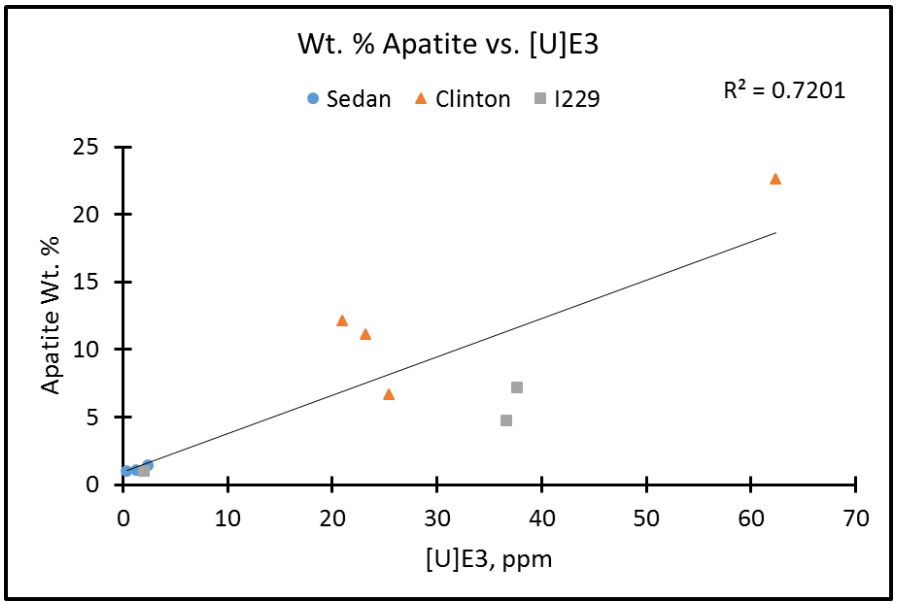

Figure 16: Wt. % apatite vs. $[U]_{E3}$. Only samples that contain >1% apatite are included. Variable levels of U enrichment of apatite at different locations and times may contribute to the data spread. The error in $[U]_{E3}$ as calculated from replicate analysis is +/- 0.04 ppm. Since no estimate of error is available for the mineral weight percentages (see section 2.4) all error for the trendline calculation is assumed to reside in the [U] concentration values.

4.1.4 F4/E4 Extractions

For both procedures the choice of reagents in the fourth step were the same, but for the E4 extraction (Heebner samples) the H_2O_2/HNO_3 aliquots were repeated several times to ensure the completeness of the reaction (Table 2). One potential issue with using H_2O_2/HNO_3 mixtures is that they oxidize both pyrite and organic matter simultaneously (Galindo et al. 2007, Tessier et al. 1979), along with uraninite (Phan et al. 2015). This does not allow the contribution of these materials to be separated. The ability of pyrite to sorb or complex U is not well established. A study by Qafoku et al. (2009) found elevated U contents in naturally occurring framboidal pyrite, which was found in both the U^{VI} and U^{IV} redox states, while Suzuki et al. (2005) found little U in framboidal pyrite from a freshwater pit of a uranium mine.

Other authors have suggested that authigenic sulfides such as pyrite are not significant sinks of U in black shale (Algeo & Maynard 2004, Galindo et al. 2007). For the Heebner samples, a cross plot of wt. % pyrite vs $[U]_{E4}$ fails to yield any correlation which suggests that pyrite is not a dominant control, or at least exhibits changeable enrichments across the samples (Figure 17). This can be contrasted with apatite, which shows a loose positive correlation (Figure 16). For future work, two viable ways by which to isolate the contribution from pyrite would be heavy liquid density separation or treatment with HF/HCl to destroy all components of the rock except kerogen and pyrite for further analysis (Ono et al. 2003, Galindo et al. 2007).

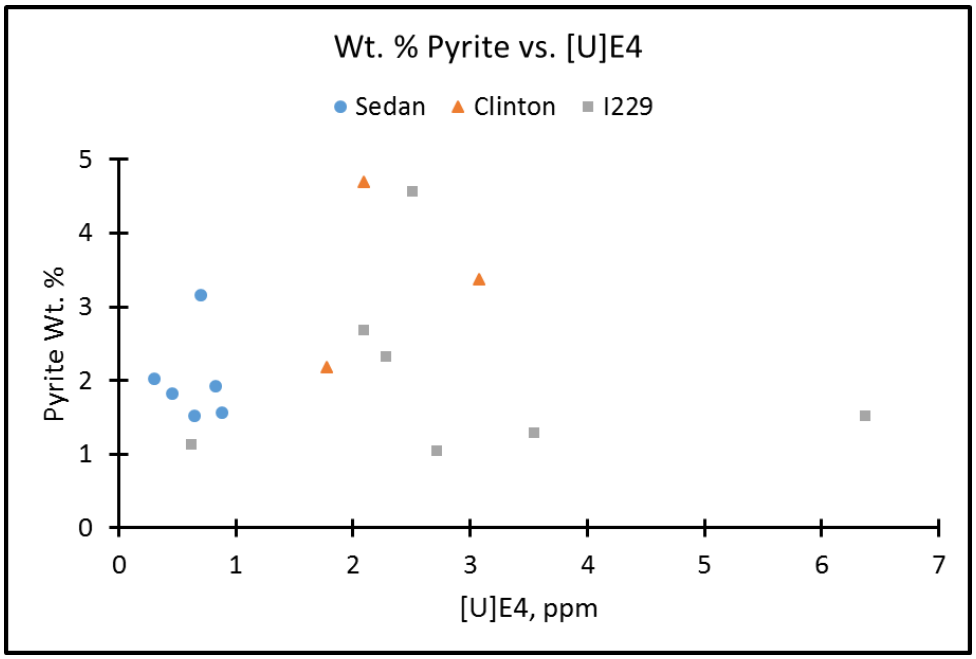

Figure 17: Wt. % pyrite vs $[U]_{E4}$. The lack of a correlation for any outcrop suggests that pyrite is not a dominant contributor to uranium in the E4 extraction. Error for [U]E4 as calculated from replicate analysis is +/- 0.20 ppm. No estimate of error is available for the mineral weight percentages (see section 2.4).

Some organic matter is able to complex with uranium (Idiz 1986, Nakashima 1992, Bednar et al. 2007, Yang et al. 2012) or influence its accumulation by driving anoxia through the consumption of oxygen during its decay (Arndt et al. 2013). In marine sediments OM is a complex mixture of many compounds. According to a review by Vandenbroucke & Largeau (2007), these compounds are often classified operationally based on their solubility into four groups: kerogen, humic acids, fulvic acids, and humin. Humic acids are a precursor to kerogen and are base-soluble, acid-insoluble, and complex with U readily (Idiz et al. 1986, Lenhart et al. 2000, Galindo et al. 2007). Additionally, humic acids may mediate biotic reduction of aqueous U^{VI} (Gu and Chen 2003). Humic acids and other soluble organics are removed in the E4 extraction (H_2O_2/HNO_3), but kerogen is not (Tessier et al. 1979, Galindo et al. 2007).

Uraninite (UO_2) is also removed in the F4/E4 extractions. Uraninite can precipitate onto organic matter, clay minerals, and pyrite under certain reducing conditions (e.g. Wersin 1994, Min et al. 2005, Phan et al. 2015, Stylo et al. 2015, Tuovinen et al. 2015). The existence of uraninite is not easily detected through bulk XRD analysis (Min et al. 2005). For future work, the presence or absence of uraninite should be verified before the sequential extractions are performed. A viable method to identify its presence is SEM analysis.

4.1.5 F5/E5 Extractions

The original sequential extraction procedures of Tessier et al. (1979) and Galindo et al. (2007) included a final total digest using peroxide fusion or multi-acid mixtures (i.e. $HCl/HNO_3/HF$). Due to equipment limitations and safety considerations regarding the use of HF, a total digest was not possible and was replaced by a hotplate aqua regia digestion. Aqua regia digestion can leave behind an amount of refractory organic matter and resistant minerals (Chen & Ma 2001), but it is considered a viable way to isolate the important "authigenic" components since it is capable of digesting phosphates, sulfides, carbonates, and less resistant organic matter (Xu et al. 2012). Since all of these materials should have been removed in the preceding extractions (F1-F4), the final aqua regia digestion can help to ascertain if those extractions were effective or if there are any remaining U-bearing materials.

It is clear from the results in Figure 5 for the Permian shale and SBC-1 and Figures 6-8 for the Heebner samples that a significant amount of U was released in the final aqua regia digestion (F5, E5). The only detected mineral that is affected in this step is chlorite (Figure 9). Any remaining refractory organic matter (kerogen) would be also be partially degraded given the oxidizing nature of aqua regia. Chlorite can adsorb U followed by reduction to precipitate nanocrystalline uranium oxides along its edges in organic-rich sediment (Bonnetti et al. 2015). It has also been shown in laboratory sorption/desorption tests by Singer et al. (2009) that chlorite can adsorb significant amounts of U^{VI} as inner-sphere complexes under short term conditions. Under longer term anaerobic conditons, the U was primarily associated with amorphous, poorly crystalline UO_2 that concentrated on chlorite edges. It is predicted that chlorite-associated UO_2 would be susceptible to the H_2O_2 leaching of the previous F4/E4 extractions similar to crystalline UO_2.

There is no correlation between chlorite intensity and $[U]_{E5}$ (Figure 18), which suggests that it is not directly (or consistently) responsible for the U released during the E5 extraction. However, it is notable that the outcrops groups cluster in different parts of the plot. This is mainly the result of a distinct trend in $[U]_{E5}$ between the outcrops, where the Sedan samples contained the least in the E5 extracts and the I229 sample set contained the most, with the Clinton samples intermediate. Since $[U]_{E5}$ is not correlative with the abundances of any of the detected minerals, a plausible explanation is that the U released in this step was released from kerogen. Kerogen would be at least partially oxidized since aqua regia is made using concentrated HNO_3. The relationship of U and kerogen is uncertain: the study of Galindo et al. (2007) found that for the Timahdit black shale of Morrocco, pyrite and kerogen together accounted for no more than 3% of the total U, which would imply that both kerogen and pyrite are not a significant carriers of uranium. However, the kerogen type of the Timahdit shale is mixed type I/II (Ambles et al. 1987), while the LPMS shales have large amounts of terrestrially-derived type III kerogens (Algeo et al. 2008). Since terrestrial OM is known to be generally more refractory (Arndt et al. 2013), and the flux of this material in the LPMS came from the paleo-North/Northeast (Coveney et al. 1987, Schultz & Coveney 1992, Hatch & Leventhal 1992), this could explain the spatial trend in $[U]_{E5}$.

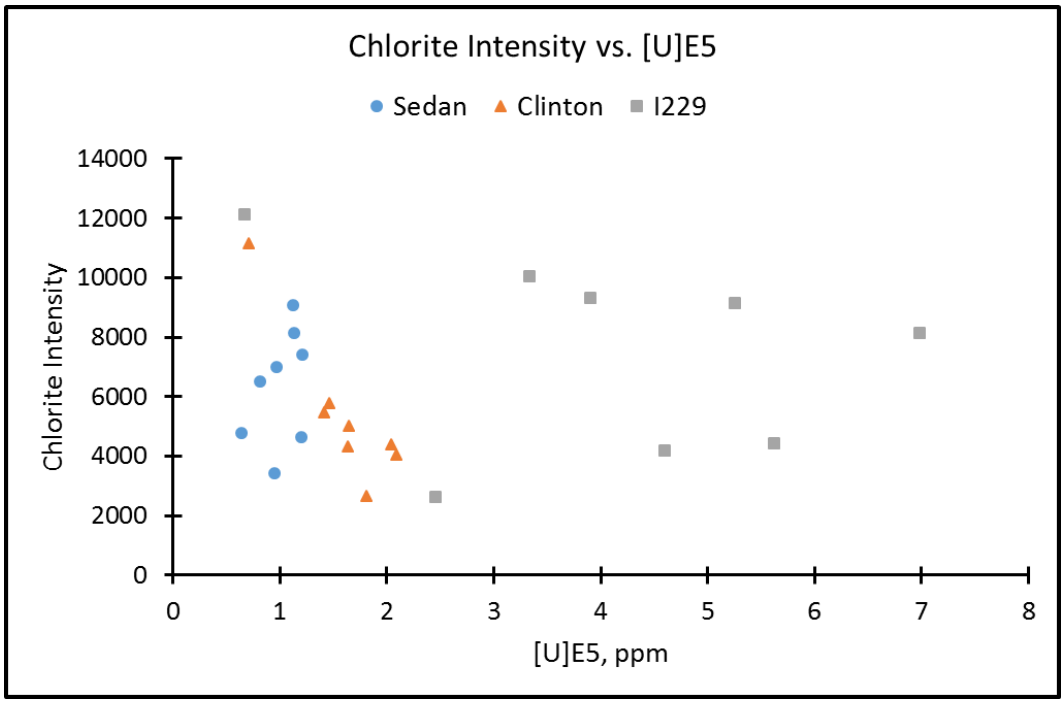

Figure 18: Chlorite intensity vs. $[U]_{E5}$. The poor correlation between suggests that chlorite does not drive the [U] content of this fraction, or does so inconsistently. The error in $[U]_{E5}$, as calculated by replicate analysis, is +/- 0.12 ppm. No error estimation is available for chlorite intensity (see section 2.4).

Both the standard Tessier method (total digest) and the alternative aqua regia digest do not allow for a discreet quantification of how much U is contained in kerogen left behind after the F4/E4 extractions (H_2O_2/HNO_3). A full digest would include the contribution from silicates, and aqua regia only partially destroys some types of organics (Chen & Ma 2001). For the Heebner samples, an amount of paraffin-like organic matter was left behind after the E5 extraction. An estimation of this material's contribution to the total U of the sample can be estimated from the difference between the total recovery from the separate ashing/microwave digestion and the total recovered from the sequential extraction (this difference is termed $[U]_k$ for convenience, and is shown in Figures 6-8 as a dashed line).

The $[U]_k$ calculation is based on the assumption that a substantial amount of U was not leached from the silicate matrix during microwave digestion, so that the only additional material that was digested comparative to the sequential extraction was refractory organics. This assumption is plausible given the minimal dissolution of the detected silicates in aqua regia (Figures 9 and 10), even with microwave digestion (Chen & Ma 2001). Additionally, the amount of U in common silicates (illite, kaolinite, quartz) are generally low, hence the low U content of a typical "detrital background" (Tribovillard & Algeo 2006). The contribution of this background likely approaches the value of an "average shale" (i.e. ~2.8 ppm U, McLennan 2001).

If the detected silicates were partially digested during the microwave digestion, the U contribution from these materials would likely be uniform across the samples since their silicate composition is fairly consistent, and so this would not easily explain sample variance in $[U]_{E5}$ or $[U]_k$. However, the values represented by $[U]_k$ are suspect due to the very close association with high apatite samples, which may indicate a sample heterogeneity effect (i.e. the inclusion of more apatite flakes) since separate and smaller (0.1g) samples were used for the microwave digest. Even so, the recovery from the microwave digest is uniformly higher even for samples with negligible apatite content, so it is apparent that an amount of U is being released from either resistant kerogen or the silicate matrix. This amount is generally small (for non-apatite containing samples). However, if the U released during extraction E5 was from kerogen (which is plausible given the poor chlorite/$[U]_{E5}$ correlation), it could be said that refractory organics can be a significant carrier of U. This result is important because a standard sequential extraction would attribute this contribution to the "residual" non-organic material, such as silicates. A means by which to isolate the contribution from chlorite and kerogen would be the insertion of a dilute HCl digestion after the E4 extraction to dissolve chlorite (Hamer et al. 2003) followed by an ashing/aqua regia digestion to destroy and dissolve any residual organics.

Outside of refractory organics, the importance of any material that is not completely digested by either hotplate aqua regia digestion or ashing/microwave-assisted aqua regia digestion (i.e. silicates and resistant oxides) depends on the particular minerals present and the goals of the study. According to Figures 9-11, several materials remain unaffected after hotplate aqua regia digestion: illite, kaolinite, rutile, anatase, and quartz – all of which are generally detrital components. Authigenic components are more valuable for paleoredox studies since they are formed in the environment in question (Tribovillard & Algeo 2006). In this respect, aqua regia digestion can have an advantage over total bulk digests by minimizing the detrital contribution. In TOC-rich shale, the detrital contribution to the redox-sensitive trace metal inventory is likely minor or subordinate to the authigenic component. For a TOC-poor "average" shale, the concentration of trace elements would approach the average of the detrital source terrane (Tribovillard & Algeo 2006) – an "average" shale contains ~3 ppm U (McLennan 2001).

The influence of detrital U can be seen in that the total U recovery for the reference shale (SBC-1) by both the sequential extraction and separate microwave-assisted digestion was below the listed value of 5.76 ppm (Table 4). This discrepancy is attributable to the contribution (<3.13 ppm) from the detrital background consisting of quartz, kaolinite, illite, rutile, and anatase. In particular, SBC-1 contains 3.4% rutile by weight, which can be U-enriched (Meinhold 2010) and is not readily digested by aqua regia or even more complete multi-acid mixtures (Xu et al. 2012). Typical U concentrations in rutile range between 3 and 130 ppm, with higher enrichments in high-grade metamorphic rocks (Meinhold 2010). A mass balance suggests that if the rutile contained ~100 ppm U, the discrepancy between the microwave-assisted digestion and the listed value could be made up by that component alone, disregarding the contribution from the other resistant minerals that compose the detrital background. The Heebner samples did not contain any known U-rich detrital minerals.

4.2 URANIUM ACCUMULATION PATTERNS IN THE HEEBNER

As seen in Figures 6-8, the distribution of uranium between the E2-E5 fractions is highly variable even across small intervals. The sequential extraction affords the opportunity to analyze the sample beyond bulk values, which can gloss over important trends. In order to compare the distributions between outcrops according to the nitrogen isotope excursions, it is assumed that these represent synchronous events.

The prevailing model for the nitrogen excursions relates them to pulses of denitrified water into the LPMS from the Panthallassic Ocean (Algeo et al. 2008), which implies that the outcrop locations would be exposed to this water mass (and record its $\delta^{15}N$ signature) approximately simultaneously. This is supported by the similar positioning of other phenomenon relative to the excursions at each outcrop (such as %C and apatite peaks). There is some variation in their position shape, which may be related to differential sedimentation rates.

4.2.1 Apatite U

Apatite is the primary U-bearing fraction when present in appreciable amounts (>1%). The abundance and associated U peaks occur on the falling limb or the termination of the nitrogen excursion at each outcrop, but there are notably different levels of enrichment at each location (Figures 6-8 and 12-14). Within the sampled intervals, the Sedan outcrop contains the least amount of apatite and apatite-associated U, while the Clinton outcrop has the most. The I229 outcrop has one enriched interval that is relatively narrow.

This spatial trend may have significance for the superestuarine circulation model and the hypothesis of upwelling on the midcontinent shelf. The formation of authigenic apatite requires supersaturation of P in sediment pore water, and is affected by other factors such as alkalinity, pH, eH, and bacterial activity (Tribovillard et al. 2015). Supersaturation often occurs in zones of upwelling where primary productivity and OM delivery to the sediment is high, but can also result from redox cycling.

Apatite accumulation by redox cycling occurs when there are fluctuations in the redox state of the water column (i.e. euxinic to anoxic, or anoxic to suboxic). Under oxic conditions, P is brought to (and fixed in) the sediment by complexation with Fe-oxides and settling OM (Filippelli 2011). Under euxinic or anoxic conditions, Fe-oxides are reduced and dissolved when they come into contact with a reducing zone in the water column or at the sediment-water interface. This causes P to be recycled back into the water column (Saltzman 2005, Slomp & Van Capellan 2007, März 2008). This can create a positive feedback loop with anoxia when the recycled P fuels primary productivity in the water column. When the feedback loop is broken by a fluctuation in redox state within the water column or at the sediment-water interface, more P can be retained by the sediment (Filippelli 2011), and may accumulate rapidly (März 2008).

Geochemical evidence of these fluctuations may be difficult to detect due to their short term duration (März 2008), and this difficulty is compounded by the affinity of authigenic apatite for many redox sensitive metals (Tribovillard et al. 2006) which might otherwise record the temporary diminishment of reducing conditions. The record of this event may also be obscured by a time averaging effect due to the low sedimentation rates that characteristic of authigenic apatite accumulation (Algeo & Heckel 2008).

Upwelling has been suggested to have occurred along the southern margin of the LPMS, which brought nutrients into the photic zone and stimulated primary productivity which in turn encouraged the development of anoxia across the shelf (Heckel 1977, Yang et al. 2003). This same upwelling model has been invoked to describe the origin of phosphatic nodules in LPMS black shales (Kidder 1985, Ece 1990). In the model of Kidder (1985), upwelling caused increased OM flux to the sediment, where it decayed and released P into interstitial pore water to eventually precipitate as apatite. If this model is correct, it would be expected that greater amounts of apatite would be found near the area of upwelling.

The paleo-location of the Sedan outcrop is proximal to the upwelling belt proposed by Yang et al. (2003). The data presented here shows that both %C and apatite abundance are lowest in the Sedan samples. The trace element enrichment patterns noted by other studies are also not consistent with strong upwelling along the southern margin since enrichment levels generally increase towards the paleo-North/Northeast (Coveney et al. 1991, Schultz & Coveney 1992, Algeo et al. 1997, Hoffman et al. 1998, Cruse and Lyons 2004, Herrmann et al. 2015). Apatite abundance and total uranium are highest for the Clinton outcrop samples. Unless the locus of upwelling was actually closer to the Clinton outcrop (which is unlikely given its distance from the shoreline) another explanation must be invoked that is consistent with the observed data and trends.

Since upwelling may not be the driving force of authigenic apatite formation, the redox cycling model offers a viable alternative explanation. The model has been invoked to describe the precipitation of phosphatic minerals in the LPMS by Hoffman et al. (1998). Algeo et al. (2004) described an interval of maximum apatite accumulation slightly above the maximum flooding surface in an LPMS shale (the Hushpuckney shale). This phosphatic interval marks a switch from terrestrial to marine organics and a transition from euxinic to fluctuating anoxic conditions. Algeo et al. (2004) called this interval a “regressive condensation surface” and attributed it to climactic drying which led to the diminishment of coastal coal swamps (the source of terrestrial OM), a weakening of the runoff-induced halocline, and increased winds and wave action that led to periodic vertical mixing of the water column. The position of the apatite peaks noted in the study units are consistent with the regressive condensation surface described by Algeo et al. (2004).

The weakening of the halocline due to decreased freshwater runoff would presumably cause the intensity of water column stratification to waver at the limits of its extent, which would lead to redox fluctuations in this fringe area and possibly enhanced apatite precipitation by redox cycling. This model is consistent with the superestaurine circulation model that

describes a halocline originating from the paleo-North/Northeast that graded into a thermocline in the Southern regions (Algeo & Heckel 2008). In the Southern region (i.e. the Sedan outcrop), this thermocline may have created a weak but *persistent* stratification of the water column that maintained black shale deposition away from the halocline. The I229 outcrop was closer to the origin of the halocline and thus experienced strong and persistent stratification. Finally, the Clinton outcrop was at the fringe of the halocline, and experienced fluctuating redox conditions due to variations in its strength or extent. This may be additionally supported by the staggered precipitation of pyrite at the Clinton location (Figure 13).

Since authigenic apatite accumulation is also favored when sedimentation rates are slow, it can be inferred that the Clinton location was the most sediment starved. This interpretation is plausible given the distance from the paleo-shoreline (Figure 1). The source of P required for apatite deposition likely came from the North/Northeast due to the poor enrichment at the Sedan outcrop. The P may have been released from remineralized OM or dissolved P that would likely characterize acidic humic-rich nearshore waters, which could then be washed out to more distal settings (Ece 1990) such as like the Clinton location.

The association between slow sediment rate, redox fluctuations, phosphatic condensation, and U accumulation in black shale has been noted by Fisher & Wignall (2000). In their study, they found that apatite precipitation concentrated on the tops and bottoms of persistently euxinic facies rather than within them (based on analysis of biofacies, degree of pyritization, framboidal pyrite size, francolite content, and elemental data). Consequently, uranium was enriched in apatite intervals that mark brief fluctuations in water column redox state rather than the most persistently anoxic intervals.

In summary, the trend in apatite deposition is supportive of the prevailing superestuarine circulation model, but not of the upwelling hypothesis. The main phosphatic surface (the “regressive condensation surface”) and the associated uranium enrichment occur predictably in all three outcrops and are linked to climactic changes, sedimentation rate, and the location’s position relative to the shoreline. This result is pertinent to uranium enrichment redox proxies since areas of phosphogenesis will incur greater uranium enrichment as a function of *fluctuating* redox conditions rather than persistent anoxia. This effect would lead to an overestimation of anoxia inferred solely from U enrichment, and underestimation of sulfidic conditions inferred from Mo/U covariation.

4.2.2 Organic U

As discussed in Section 5.1, organic matter is important for U accumulation both indirectly and indirectly, but the selectivity of both sequential extractions (Table 1, Table 2) for OM are poor since contributions from pyrite, chlorite, and uraninite are potentially mixed in. Qualitatively it appears that pyrite and chlorite are not directly or consistently responsible for driving U accumulation in the Heebner (Figures 17 and 18), but the potential influence of uraninite is not clear.

It is noteworthy to point out that the peaks in $[U]_{E4}$ coincide with the larger peaks in %C that occur after the termination of the nitrogen excursion in all three outcrops (Figures 6-8). In general, $[U]_{E4}$ tracks %C (except where carbonate content is significant). In particular, the larger %C peaks at the Clinton and I229 outcrops are associated with large spikes in $[U]_{E4}$. A similar peak in TOC was described by Algeo et al. (2004), and was found to be a maximum of terrestrial organics that resulted from a peak in humid conditions, runoff, and inundation of nearshore coal swamps.

This description is consistent with the smaller observed %C maxima at the Sedan outcrop at the same horizon, due to the Sedan location's greater distance from the terrestrial flux from the paleo-North/Northeast. It is unclear if the $[U]_{E4}$ peaks are the result of indirect uraninite precipitation in association with the abundant organic matter, redox conditions during maximum flooding, or direct association with terrestrial OM. Interpretation in this area is hampered by the low sampling density.

Algeo & Maynard (2004) proposed that uranium accumulation in black shale occurs primarily by direct complexation with organic matter within a low-mid TOC range, but as TOC exceeds a certain threshold, euxinic conditions predominate and U accumulation is driven by the precipitation of U-bearing authigenic minerals (such as uraninite) in association with sulfides. Their hypothesis is supported by a degradation of the TOC-U relationship above a certain threshold in several LPMS shales (Algeo & Maynard 2004). To date no studies have attempted to directly identify uraninite in the LPMS shales, which often requires techniques such as electron microscopy (Min et al. 2005) or EXAFS (Bargar et al. 2008).

While there is a lack of studies that directly compare the influence of organic matter type on U complexation or uraninite precipitation, there is some evidence that terrestrial OM has a particular affinity. Landais (1995) suggested that most ore-grade sandstone-hosted uranium deposits contain type III kerogen, and Leventhal (1981) demonstrated that for Appalachian Devonian black shales there is a positive correlation between vitrinite and U content. Nakashima (1992) demonstrated in a laboratory study that terrestrial organic materials such as lignite and peat have the ability to rapidly and irreversibly form organometallic complexes with U, and these complexes have been described in natural lignite deposits (Mohan et al. 1991, Ilger et al. 1987, Arbuzov et al. 2012, Lidman et al. 2013). With diagenesis and thermal maturation, lignite tends to release U to precipitate finely disseminated uraninite in coal (Meuneir et al. 1990).

The ambiguity with regards to U accumulation and organic matter type requires more direct methods to resolve. This relationship would be relevant to redox studies if different types of OM exhibited significantly variable abilities to complex U or facilitate the precipitation of uraninite. The identification of uraninite and its distribution (if present) in various black shales would be beneficial.

4.2.3 Carbonate U

Carbonates contributed small amounts of uranium to the bulk content of the samples (average 1.08 ppm, SD 0.76), although this amount can be a large proportion of total U in less enriched samples. There appears to be covariation with the nitrogen excursions in the Sedan and Clinton outcrops, and possibly in the I229 outcrop. The peak accumulation of carbonate minerals at the nitrogen excursion peaks may be indicative of enhanced sedimentary denitrification during the excursions due to the ability of denitrifying bacteria to facilitate carbonate precipitation (Martin et al. 2013, Erşan 2015, Riding 2000). The origin of the carbonate is presumably authigenic; minerals such as calcite, dolomite, and siderite tend to form in association with sulfate and Fe-reduction during early diagenesis in organic sediments (Schrag et al. 2013). This is partially supported by covariation with the estimated abundance of pyrite in the I229 and Clinton outcrops, but not in the Sedan.

The total wt. % of carbonate minerals (dolomite wt.% + calcite wt.%) vs. $[U]_{E2}$ fails to elucidate a correlation (Figure 15), which suggests changeable enrichment of carbonate minerals. However, individual plots (dolomite vs $[U]_{E2}$ and calcite vs. $[U]_{E2}$) show that dolomite exhibits a positive correlation (Figure 15), with the implication that it is more enriched than calcite and contributes more to the total value of $[U]_{E2}$. A crossplot of $[U]_{E2}$ vs $[U]_{E4}$ (Figure 15) also reveals a positive relationship between these two fractions, with the exception of three outlier data points that occur during the largest peaks in %C at the Clinton and I229 outcrops. An explanation for this correlation may be that during diagenesis an amount of U-bearing organic compounds are degraded, and the released U is incorporated into dolomite as it crystallizes.

4.3 IMPLICATIONS FOR THE USE OF URANIUM REDOX PROXIES IN BLACK SHALE

4.3.1 U ENRICHMENT FACTORS

A common use of uranium for redox studies is to analyze concentration trends (e.g. Hatch & Leventhal 1992, Hoffman et al. 1998, Algeo & Maynard 2004, Schroder & Grotzinger 2007, Chun et al. 2010, Palike et al. 2014, Takahashi et al. 2015). Since U is reduced to a particle-reactive tetravalent state under reducing conditions (Anderson 1989, Barnes & Cochran 1990, Klinkhammer & Palmer 1991, Ivanovich & Harmon 1992, Swarzenski et al. 1999), a greater concentration of U is expected to accumulate during intervals that represent anoxic conditions in the sediment or water column. These concentrations are often presented as “enrichment factors”, where the values are normalized to aluminum and compared to the values for an “average” shale (Algeo & Tribovillard 2006). U concentrations are particularly valuable when compared with other redox sensitive metals such as Ni, Cu, Mo, and V, which exhibit slightly different behaviors (Algeo & Tribovillard 2006). For example, Mo tends to accumulate in the sediment at a quicker rate compared to U under euxinic conditions (relative to non-sulfidic anoxic conditions). This pattern allows for the development of euxinia to be identified by Mo/U ratios (Algeo & Tribovillard 2006).

The redox-cycling mode of apatite accumulation appears to be responsible for a substantial portion of U accumulation in the LPMS-type shales. As described in the previous section, the precipitation of authigenic apatite (most notably the prominent "regressive condensation surface") is related to fluctuating redox conditions in the water column and slow sedimentation rates. These two variables have a spatial dependency in relation to the distance from the shoreline. Since the resulting U enrichment is not due to persistently anoxic conditions, it can exaggerate the degree of anoxia within the analyzed section and at locations across geochemical transect where authigenic apatite accumulates.

4.3.2 $U^{238}/^{235}U$ RATIOS

A growing area of interest is the application of $^{238}U/^{235}U$ isotope ratios in paleoredox studies (e.g. Montoya-Pino et al. 2010, Brennecka et al. 2011, Asael et al. 2013, Kendall et al. 2013, Romaniello et al. 2013, Dahl et al. 2014, Holmden et al. 2015, Kendall et al. 2015). Due to improvements in MC-ICP-MS techniques, relatively small changes in $^{238}U/^{235}U$ can now be resolved (Weyer et al 2008). The $^{238}U/^{235}U$ isotope is presented as $\delta^{238}U$, which is defined as:

$$\delta 238\mathrm{U} = \left(\frac{238\mathrm{U}/235\mathrm{U})_{sample}}{(238\mathrm{U}/235\mathrm{U})_{standard}} - 1 \right) \times 1000$$

Specifics on $^{238}U/^{235}U$ fractionation, its use as a paleoredox proxy, and the current state of the research is described in more detail in Appendix C. In short, $\delta^{238}U$ shows promise as a global-scale paleoredox proxy based on a nuclear-volume induced (Schauble 2007) fractionation in reducing sediment (Andersen et al. 2015). Theoretically, $^{238}U/^{235}U$ ratios in open marine deposits can record oceanic drawdown in ^{238}U during the expansion of anoxic sinks at a global level (Montoya-Pino et al. 2010).

Recent work has implicated the role of biotic reduction in ^{238}U-enriched fractionation (Basu et al. 2014, Stylo et al. 2015). It has been shown that the concentration of non-carbonate uranyl species in pore water is the primary control on bioreduction rates of uranium (Belli et al. 2015). Belli et al. (2015) found that the presence of dissolved inorganic carbon, Ca^{2+}, and Mg^{2+} suppressed the formation of non-carbonate uranyl species and limited the rate of bioreduction. Bioavailable forms of uranyl species include hydroxide, hydrated, and certain organic varieties (Belli et al. 2015).

The high concentration of U in authigenic apatite suggests that its accumulation could substantially affect $\delta^{238}U$ values if it is associated with a notable fractionation. Uranium in phosphorite deposits can be found in both U^{VI} and U^{IV} forms (Soudry et al. 2002), but within reducing laminated organic-rich sediments the oxidation state is usually U^{IV} unless exposed subaerially (Jarvis et al. 1994, Soudry et al. 2002). The precipitation of authigenic apatite is often mediated or directly precipitated by sulfate-reducing bacteria (Goldhammer et al. 2010, Tribovillard 2010, Berndmeyer et al. 2012, Hiatt et al. 2015), and some sulfate-reducing bacteria can reduce uranium (Lovley & Phillips 1991).

If apatite incorporates uranium that was bioreduced by sulfate reducing bacteria or another reductive biotic process, it might incur a positive ^{238}U fractionation if the system was open given the association between heavy $\delta^{238}U$ values and biotic reduction (Stylo et al. 2015, Basu et al. 2014). In this case, the impact on the $^{238}U/^{235}U$ paleoredox proxy would be similar to that of the U-enrichment based proxy, where the inferred intensity of anoxic conditions would be overestimated.

Romaniello et al. (2013) found that primary carbonate precipitates recorded seawater-like $^{238}U/^{235}U$ values. This signal was not maintained in bulk carbonate sediments, which recorded heavier $^{238}U/^{235}U$ values. The data in Figure 15 shows that U accumulation in carbonates is related to U concentration in the $[U]_{E4}$ fraction (OM, pyrite, uraninite). A plausible interpretation is that carbonates incorporate U that is released from the $[U]_{E4}$ associated materials during diagenesis. The carbonate isotopic signal may reflect the composition of the $[U]_{E4}$ fraction materials in impure carbonate sediments rather than that of seawater.

CONCLUSIONS

Sequential extractions are viable way to identify and quantify U-bearing materials within samples and to establish how U distribution varies across depositional systems. This technique can be used to help identify the action of local processes that need to be considered for redox analysis. Common sequential extraction procedures will likely need modifications that depend on the sample composition; some preliminary information (obtained through methods such as XRD, SEM, and petrographic microscope analysis) should be collected before designing the extraction.

In the case of the LPMS shales and other phosphatic sediments, common sequential extractions are inadequate and require an additional step such as a dilute HNO_3 extraction. U-enriched apatite may accumulate as the result of redox fluctuations and would exaggerate the intensity of anoxia based on the U concentrations. The $^{238}U/^{235}U$ proxy might be affected similarly if the U that is incorporated by apatite was from a bio-reduced pool. The spatial trend in apatite accumulation and U are supportive of the prevailing superestuarine circulation model that invokes the presence of a halocline, but does not support the existence of an upwelling belt along the Southern margin of the system.

Future work in this area should concentrate on identifying whether uraninite is present in the LPMS shales and how it is distributed in relation to other constituents. The influence of pyrite and OM type on U accumulation are also areas that require more attention, and may be relevant to the successful application of U and other trace metal paleoredox proxies.

REFERENCES

Adlis, David S., et al. "Isotope stratigraphy and paleodepth changes of Pennsylvanian cyclical sedimentary deposits." *Palaios* (1988): 487-506.

Algeo, Thomas J., et al. "Changes in ocean denitrification during Late Carboniferous glacial–interglacial cycles." Nature Geoscience 1.10 (2008): 709-714.

Algeo, Thomas J., and Philip H. Heckel. "The Late Pennsylvanian midcontinent sea of North America: a review." *Palaeogeography, Palaeoclimatology, Palaeoecology* 268.3 (2008): 205-221.

Algeo, Thomas J., and J. Barry Maynard. "Trace-element behavior and redox facies in core shales of Upper Pennsylvanian Kansas-type cyclothems. "*Chemical geology* 206.3 (2004): 289-318.

Algeo, Thomas J., and J. Barry Maynard. "Trace-metal covariation as a guide to water-mass conditions in ancient anoxic marine environments." *Geosphere*4.5 (2008): 872-887.

Algeo, Thomas J., Lorenz Schwark, and James C. Hower. "High-resolution geochemistry and sequence stratigraphy of the Hushpuckney Shale (Swope Formation, eastern Kansas): implications for climato-environmental dynamics of the Late Pennsylvanian Midcontinent Seaway." *Chemical Geology* 206.3 (2004): 259-288.

Algeo, Thomas J., and N. Tribovillard. "Environmental analysis of paleoceanographic systems based on molybdenum–uranium covariation." *Chemical Geology* 268.3 (2009): 211-225.

Alvarez, Mónica B., et al. "Chemometric approach to visualize and easily interpret data from sequential extraction procedures applied to sediment samples." *Journal of hazardous materials* 274 (2014): 455-464.

Ambles, André, Germaine Dupas, and Jean-Claude Jacquesy. "Solubilization of Timahdit (Morocco) oil shale kerogen catalysed by 18-Crown-6." *Tetrahedron letters* 28.51 (1987): 6449-6452.

Andersen, M. B., et al. "A modern framework for the interpretation of 238 U/235 U in studies of ancient ocean redox." *Earth and Planetary Science Letters* 400 (2014): 184-194.

Anderson, Robert F., Martin Q. Fleisher, and Anne P. LeHuray. "Concentration, oxidation state, and particulate flux of uranium in the Black Sea." *Geochimica et Cosmochimica Acta* 53.9 (1989): 2215-2224.

Arain, M. B., et al. "Comparison of different extraction approaches for heavy metal partitioning in sediment samples." *Pedosphere* 19.4 (2009): 476-485.

Arbuzov, S. I., et al. "Modes of occurrence of uranium and thorium in coals and peats of Northern Asia." *Solid Fuel Chemistry* 46.1 (2012): 52-66.

Arthur, Michael A., and Bradley B. Sageman. "Marine shales: depositional mechanisms and environments of ancient deposits." *Annual Review of Earth and Planetary Sciences* 22 (1994): 499-551.

Asael, Dan, et al. "Coupled molybdenum, iron and uranium stable isotopes as oceanic paleoredox proxies during the Paleoproterozoic Shunga Event."*Chemical Geology* 362 (2013): 193-210.

Bacon, Jeffrey R., Irene J. Hewitt, and Patricia Cooper. "Reproducibility of the BCR sequential extraction procedure in a long-term study of the association of heavy metals with soil components in an upland catchment in Scotland."*Science of the Total Environment* 337.1 (2005): 191-205.

Bargar, John R., et al. "Biogenic uraninite nanoparticles and their importance for uranium remediation." *Elements* 4.6 (2008): 407-412.

Barnes, C. E., and J. K. Cochran. "Uranium removal in oceanic sediments and the oceanic U balance." *Earth and Planetary Science Letters* 97.1 (1990): 94-101.

Basu, Anirban, et al. "Uranium isotopic fractionation factors during U (VI) reduction by bacterial isolates." *Geochimica et Cosmochimica Acta* 136 (2014): 100-113.

Bednar, A. J., et al. "Effects of organic matter on the distribution of uranium in soil and plant matrices." *Chemosphere* 70.2 (2007): 237-247.

Belli, Keaton M., et al. "Effects of aqueous uranyl speciation on the kinetics of microbial uranium reduction." *Geochimica et Cosmochimica Acta* 157 (2015): 109-124.

Benmore, Richard A., Max L. Coleman, and John M. McArthur. "Origin of sedimentary francolite from its sulphur and carbon isotope composition." (1983): 516-518.

Berndmeyer, C., et al. "The influence of bacterial activity on phosphorite formation in the Miocene Monterey Formation, California." *Palaeogeography, Palaeoclimatology, Palaeoecology* 317 (2012): 171-181.

Bonis, N. R., Micha Ruhl, and W. M. Kürschner. "Climate change driven black shale deposition during the end-Triassic in the western Tethys."*Palaeogeography, Palaeoclimatology, Palaeoecology* 290.1 (2010): 151-159.

Bonnetti, Christophe, et al. "The Nuheting deposit, Erlian Basin, NE China: Synsedimentary to diagenetic uranium mineralization." *Ore Geology Reviews*69 (2015): 118-139.

Brennecka, Gregory A., et al. "Rapid expansion of oceanic anoxia immediately before the end-Permian mass extinction." *Proceedings of the National Academy of Sciences* 108.43 (2011): 17631-17634.

Cecil, C. Blaine. "Climate controls on the stratigraphy of a Middle Pennsylvanian cyclothem in North America." (2003).

Cecil, C. Blaine, William A. DiMichele, and Scott D. Elrick. "Middle and Late Pennsylvanian cyclothems, American Midcontinent: Ice-age environmental changes and terrestrial biotic dynamics." *Comptes Rendus Geoscience* 346.7 (2014): 159-168.

Chermak, John A., and Madeline E. Schreiber. "Mineralogy and trace element geochemistry of gas shales in the United States: Environmental implications."*International Journal of Coal Geology* 126 (2014): 32-44.

Chun, Cecily OJ, Margaret L. Delaney, and James C. Zachos. "Paleoredox changes across the Paleocene-Eocene thermal maximum, Walvis Ridge (ODP Sites 1262, 1263, and 1266): Evidence from Mn and U enrichment factors."*Paleoceanography* 25.4 (2010).

Coveney, Raymond M., et al. "Origins of metals and organic matter in the Mecca Quarry Shale Member and stratigraphically equivalent beds across the Midwest." Economic Geology 82.4 (1987): 915-933.

Coveney, Raymond M., and Michael D. Glascock. "A review of the origins of metal-rich Pennsylvanian black shales, central USA, with an inferred role for basinal brines." Applied Geochemistry 4.4 (1989): 347-367.

Coveney, Raymond M., W. Lynn Watney, and Christopher G. Maples. "Contrasting depositional models for Pennsylvanian black shale discerned from molybdenum abundances." *Geology* 19.2 (1991): 147-150.

Cruse, Anna M., and Timothy W. Lyons. "Trace metal records of regional paleoenvironmental variability in Pennsylvanian (Upper Carboniferous) black shales." *Chemical Geology* 206.3 (2004): 319-345.

Dahl, Tais W., et al. "Uranium isotopes distinguish two geochemically distinct stages during the later Cambrian SPICE event." *Earth and planetary science letters* 401 (2014): 313-326.

Desborough, G. A., J. R. Hatch, and J. S. Leventhal. "Geochemical and mineralogical comparison of the Upper Pennsylvanian Stark Shale Member of the Dennis Limestone, East-central Kansas, with the Middle Pennsylvanian Mecca Quarry Shale Member of the Carbondale Formation in Illinois and the Linton Formation in Indiana." *US Geol. Surv. Circ* 1058 (1991): 12-30.

Doveton, J. H., and D. F. Merriam. "Borehole petrophysical chemostratigraphy of Pennsylvanian black shales in the Kansas subsurface." *Chemical geology*206.3 (2004): 249-258.

Ece, Omer Isik. "Geochemistry and occurrence of authigenetic phosphate nodules from the Desmoinesian cyclic Excello epeiric sea of the Midcontinent, USA." *Marine and Petroleum Geology* 7.3 (1990): 298-312.

Erşan, Yusuf Çağatay, Nele de Belie, and Nico Boon. "Microbially induced CaCO 3 precipitation through denitrification: An optimization study in minimal nutrient environment." *Biochemical Engineering Journal* 101 (2015): 108-118.

Filippelli, Gabriel M. "Phosphate rock formation and marine phosphorus geochemistry: the deep time perspective." *Chemosphere* 84.6 (2011): 759-766.

Fisher, Q. J., and P. B. Wignall. "Palaeoenvironmental controls on the uranium distribution in an Upper Carboniferous black shale (Gastrioceras listeri Marine Band) and associated strata; England." *Chemical Geology* 175.3 (2001): 605-621.

Galindo, C., et al. "Distribution of naturally occurring radionuclides (U, Th) in Timahdit black shale (Morocco)." *Journal of environmental Radioactivity* 92.1 (2007): 41-54.

Goldhammer, Tobias, et al. "Microbial sequestration of phosphorus in anoxic upwelling sediments." *Nature Geoscience* 3.8 (2010): 557-561.

Gu, Baohua, and Jie Chen. "Enhanced microbial reduction of Cr (VI) and U (VI) by different natural organic matter fractions." *Geochimica et cosmochimica acta* 67.19 (2003): 3575-3582.

Hamer, M., et al. "Dissolution of ripidolite (Mg, Fe-chlorite) in organic and inorganic acid solutions." *Soil Science Society of America Journal* 67.2 (2003): 654-661.

Hatch, J. R., and J. S. Leventhal. "Relationship between inferred redox potential of the depositional environment and geochemistry of the Upper Pennsylvanian (Missourian) Stark Shale Member of the Dennis Limestone, Wabaunsee County, Kansas, USA." *Chemical Geology* 99.1 (1992): 65-82.

Heckel, P. H. "Origin of phosphatic black shale facies in Pennsylvanian cyclothems of mid-continent North America." *AAPG Bulletin* 61.7 (1977): 1045-1068.

Heckel, P. H. "Thin widespread Pennsylvanian black shales of Midcontinent North America: a record of a cyclic succession of widespread pycnoclines in a fluctuating epeiric sea." *Geological Society, London, Special Publications* 58.1 (1991): 259-273.

Heckel, Philip H. "Pennsylvanian cyclothems in Midcontinent North America as far-field effects of waxing and waning of Gondwana ice sheets." *Geological Society of America Special Papers* 441 (2008): 275-289.

Herrmann, Achim D., et al. "Anomalous molybdenum isotope trends in Upper Pennsylvanian euxinic facies: Significance for use of δ 98 Mo as a global marine redox proxy." Chemical Geology 324 (2012): 87-98.

Herrmann, Achim D., James E. Barrick, and Thomas J. Algeo. "The relationship of conodont biofacies to spatially variable water mass properties in the Late Pennsylvanian Midcontinent Sea." *Paleoceanography* 30.3 (2015): 269-283.

Hiatt, Eric E., Peir K. Pufahl, and Cole T. Edwards. "Sedimentary phosphate and associated fossil bacteria in a Paleoproterozoic tidal flat in the 1.85 Ga Michigamme Formation, Michigan, USA." *Sedimentary Geology* 319 (2015): 24-39.

Hoffman, D. L., et al. "Regional and stratigraphic variation in bottomwater anoxia in offshore core shales of Upper Pennsylvanian cyclothems from the Eastern Midcontinent Shelf (Kansas), USA." (1998): 243-269.

Holmden, C., M. Amini, and R. Francois. "Uranium isotope fractionation in Saanich Inlet: A modern analog study of a paleoredox tracer." *Geochimica et Cosmochimica Acta* 153 (2015): 202-215.

Idiz, Erdem F., Donald Carlisle, and I. R. Kaplan. "Interaction between organic matter and trace metals in a uranium rich bog, Kern County, California, USA."*Applied geochemistry* 1.5 (1986): 573-590.

Ilger, J. Drew, et al. "Modes of occurrence of uranium in carbonaceous uranium deposits: characterization of uranium in a South Texas (USA) lignite." *Chemical geology* 63.3 (1987): 197-216.

Ivanovich, Miro, and Russell S. Harmon. "Uranium-series disequilibrium: applications to earth, marine, and environmental sciences. 2." (1992).

Joachimski, Michael M., and Lance L. Lambert. "Salinity contrast in the US Midcontinent Sea during Pennsylvanian glacio-eustatic highstands: evidence from conodont apatite δ 18 O." *Palaeogeography, Palaeoclimatology, Palaeoecology* (2015).

Joachimski, Michael M., Peter H. von Bitter, and Werner Buggisch. "Constraints on Pennsylvanian glacioeustatic sea-level changes using oxygen isotopes of conodont apatite." *Geology* 34.4 (2006): 277-280.

Karaca, Semra, Muammer Akyürek, and Samih Bayrakçeken. "The removal of pyritic sulfur from Aşkale lignite in aqueous suspension by nitric acid." *Fuel processing technology* 80.1 (2003): 1-8.

Kendall, Brian, et al. "Uranium isotope fractionation suggests oxidative uranium mobilization at 2.50 Ga." *Chemical Geology* 362 (2013): 105-114.

Kendall, Brian, et al. "Uranium and molybdenum isotope evidence for an episode of widespread ocean oxygenation during the late Ediacaran Period."*Geochimica et Cosmochimica Acta* 156 (2015): 173-193.

Kidder, David L. "Petrology and origin of phosphate nodules from the Midcontinent Pennsylvanian epicontinental sea." *Journal of Sedimentary Research* 55.6 (1985).

Klinkhammer, G. P., and M. R. Palmer. "Uranium in the oceans: where it goes and why." *Geochimica et Cosmochimica Acta* 55.7 (1991): 1799-1806.

Landais, P. "Organic geochemistry of sedimentary uranium ore deposits." *Ore Geology Reviews* 11.1 (1996): 33-51.

Lash, Gary G., and David R. Blood. "Organic matter accumulation, redox, and diagenetic history of the Marcellus Formation, southwestern Pennsylvania, Appalachian basin." *Marine and Petroleum Geology* 57 (2014): 244-263.

Lenhart, John J., et al. "Uranium (VI) complexation with citric, humic and fulvic acids." *Radiochimica Acta International journal for chemical aspects of nuclear science and technology* 88.6/2000 (2000): 345.

Lidman, Fredrik, et al. "Distribution and transport of radionuclides in a boreal mire–assessing past, present and future accumulation of uranium, thorium and radium." *Journal of environmental radioactivity* 121 (2013): 87-97.

Lovley, Derek R., et al. "Enzymatic iron and uranium reduction by sulfate-reducing bacteria." *Marine Geology* 113.1 (1993): 41-53.

Lüning, S., and S. Kolonic. "URNIUM SPECTRAL GAMMA-RAY RESPONSE AS AP ROXY FOR ORGANIC RICHNESS IN BLACK SHALES: APPLICABILITY AND LIMITATIONS." *Journal of petroleum geology* (2003): 153-174.

Martin, J. M., P. Nirel, and A. J. Thomas. "Sequential extraction techniques: promises and problems." *Marine Chemistry* 22.2 (1987): 313-341.

März, C., et al. "Redox sensitivity of P cycling during marine black shale formation: dynamics of sulfidic and anoxic, non-sulfidic bottom waters."*Geochimica et Cosmochimica Acta* 72.15 (2008): 3703-3717.

McClellan, G. H., and F. N. Saavedra. "Proterozoic and Cambrian phosphorites–specialist studies: chemical and mineral characteristics of some Cambrian and Precambrian phosphorites." *Phosphate deposits of the world* 1 (1986): 244-266.

McLean, J. E., and B. E. Bledsoe. "Behaviour of metals in soils (EPA Ground Water Issue, EPA 540-S-92-018: 25 pp)." *Washington, USA: Environmental Protection Agency* (1992).

McLennan, Scott M. "Relationships between the trace element composition of sedimentary rocks and upper continental crust." *Geochemistry, Geophysics, Geosystems* 2.4 (2001).

McManus, James, et al. "Authigenic uranium: relationship to oxygen penetration depth and organic carbon rain." *Geochimica et Cosmochimica Acta*69.1 (2005): 95-108.

Meinhold, Guido. "Rutile and its applications in earth sciences." *Earth-Science Reviews* 102.1 (2010): 1-28.

Meunier, J. D., P. Landais, and M. Pagel. "Experimental evidence of uraninite formation from diagenesis of uranium-rich organic matter." *Geochimica et Cosmochimica Acta* 54.3 (1990): 809-817.

Min, Maozhong, et al. "Evidence of uranium biomineralization in sandstone-hosted roll-front uranium deposits, northwestern China." *Ore Geology Reviews*26.3 (2005): 198-206.

Mohan, Mysore S., J. Drew Ilger, and Ralph A. Zingaro. "Speciation of uranium in a South Texas lignite: additional evidence for a mixed mode of occurrence."*Energy & fuels* 5.4 (1991): 568-573.

Montoya-Pino, Carolina, et al. "Global enhancement of ocean anoxia during Oceanic Anoxic Event 2: A quantitative approach using U isotopes." *Geology*38.4 (2010): 315-318.

Mossop, Katherine F., and Christine M. Davidson. "Comparison of original and modified BCR sequential extraction procedures for the fractionation of copper, iron, lead, manganese and zinc in soils and sediments." *Analytica Chimica Acta* 478.1 (2003): 111-118.

Murphy, Melissa J., et al. "Fractionation of 238 U/235 U by reduction during low temperature uranium mineralisation processes." *Earth and Planetary Science Letters* 388 (2014): 306-317.

Nakashima, Satoru. "Complexation and reduction of uranium by lignite."*Science of the total environment* 117 (1992): 425-437.

Noordmann, J., et al. "Uranium and molybdenum isotope systematics in modern euxinic basins: Case studies from the central Baltic Sea and the Kyllaren fjord (Norway)." *Chemical Geology* 396 (2015): 182-195.

Pälike, Cecily, Margaret L. Delaney, and James C. Zachos. "Deep-sea redox across the Paleocene-Eocene thermal maximum." *Geochemistry, Geophysics, Geosystems* 15.4 (2014): 1038-1053.

Partin, C. A., et al. "Large-scale fluctuations in Precambrian atmospheric and oceanic oxygen levels from the record of U in shales." *Earth and Planetary Science Letters* 369 (2013): 284-293.

Phan, Thai T., et al. "Trace metal distribution and mobility in drill cuttings and produced waters from Marcellus Shale gas extraction: Uranium, arsenic, barium." *Applied Geochemistry* (2015).

Piper, D. Z., and S. E. Calvert. "A marine biogeochemical perspective on black shale deposition." *Earth-Science Reviews* 95.1 (2009): 63-96.

Qafoku, Nikolla P., et al. "Uranium in framboidal pyrite from a naturally bioreduced alluvial sediment." *Environmental science & technology* 43.22 (2009): 8528-8534.

Quejido, A. J., et al. "Distribution of trace elements in fracture fillings from the “Mina Fe” uranium deposit (Spain) by sequential leaching: implications for the retention processes." *Applied geochemistry* 20.3 (2005): 487-506.

Quevauviller, Ph, et al. "Certification of trace metal extractable contents in a sediment reference material (CRM 601) following a three-step sequential extraction procedure." *Science of the Total Environment* 205.2 (1997): 223-234.

Rauret, G., et al. "Improvement of the BCR three step sequential extraction procedure prior to the certification of new sediment and soil reference materials." *Journal of Environmental Monitoring* 1.1 (1999): 57-61.

Riding, Robert. "Microbial carbonates: the geological record of calcified bacterial–algal mats and biofilms." *Sedimentology* 47.s1 (2000): 179-214.

Roe, Kevin K., and William C. Burnett. "Uranium geochemistry and dating of Pacific island apatite." *Geochimica et Cosmochimica Acta* 49.7 (1985): 1581-1592.

Runnels, Russell T., John A. Schleicher, and H. S. Van Nortwick. *Composition of some uranium-bearing phosphate nodules from Kansas shales*, 1953.

Ruttenberg, Kathleen C. "Development of a sequential extraction method for different forms of phosphorus in marine sediments." *Limnology and oceanography* 37.7 (1992): 1460-1482.

Salama, Walid, et al. "Microbial pathways and palaeoenvironmental conditions involved in the formation of phosphorite grains, Safaga District, Egypt."*Sedimentary Geology* 325 (2015): 41-58.

Saltzman, Matthew R. "Phosphorus, nitrogen, and the redox evolution of the Paleozoic oceans." *Geology* 33.7 (2005): 573-576.

Schovsbo, Niels H. "Uranium enrichment shorewards in black shales: a case study from the Scandinavian Alum Shale." *Gff* 124.2 (2002): 107-115.

Schrag, Daniel P., et al. "Authigenic carbonate and the history of the global carbon cycle." *science* 339.6119 (2013): 540-543.

Schröder, S., and J. P. Grotzinger. "Evidence for anoxia at the Ediacaran–Cambrian boundary: the record of redox-sensitive trace elements and rare earth elements in Oman." *Journal of the Geological Society* 164.1 (2007): 175-187.

Schultz, Richard B. "Geochemical relationships of Late Paleozoic carbon-rich shales of the Midcontinent, USA: a compendium of results advocating changeable geochemical conditions." *Chemical geology* 206.3 (2004): 347-372.

Schultz, Richard B., Raymond M. Coveney. "Time-dependent changes for Midcontinent Pennsylvania black shales, USA." *Chemical geology* 99.1 (1992): 83-100.

Singer, David M., Kate Maher, and Gordon E. Brown. "Uranyl–chlorite sorption/desorption: Evaluation of different U (VI) sequestration processes."*Geochimica et Cosmochimica Acta* 73.20 (2009): 5989-6007.

Slomp, C. P., and P. Van Cappellen. "The global marine phosphorus cycle: sensitivity to oceanic circulation." *Biogeosciences* 4 (2007): 155-171.

Soudry, David, et al. "Uranium oxidation state and related variations in geochemistry of phosphorites from the Negev (southern Israel)." *Chemical Geology* 189.3 (2002): 213-230.

Spirakis, Charles S. "The roles of organic matter in the formation of uranium deposits in sedimentary rocks." *Ore Geology Reviews* 11.1 (1996): 53-69.

Stylo, Malgorzata, et al. "Uranium isotopes fingerprint biotic reduction."*Proceedings of the National Academy of Sciences* 112.18 (2015): 5619-5624.

Suzuki, Yohey, et al. "Direct microbial reduction and subsequent preservation of uranium in natural near-surface sediment." *Applied and Environmental Microbiology* 71.4 (2005): 1790-1797.

Swarzenski, P. W., et al. "Uranium biogeochemistry across the redox transition zone of a permanently stratified fjord: Framvaren, Norway." *Marine Chemistry*67.3 (1999): 181-198.

Takahashi, Satoshi, et al. "Redox conditions in the end-Early Triassic Panthalassa." *Palaeogeography, Palaeoclimatology, Palaeoecology* 432 (2015): 15-28.

Tessier, A., GC Campbell, and M. Bisson. "Sequential extraction procedure for the speciation of particulate trace metals." *Analytical chemistry* 51.7 (1979): 844-851.

Trabucho-Alexandre, J., W. W. Hay, and P. L. De Boer. "Phanerozoic environments of black shale deposition and the Wilson Cycle." *Solid Earth* 3.1 (2012): 29-42.

Tribovillard, Nicolas, et al. "Trace metals as paleoredox and paleoproductivity proxies: an update." *Chemical Geology* 232.1 (2006): 12-32.

Tribovillard, Nicolas, et al. "Analysis of marine environmental conditions based on molybdenum–uranium covariation—Applications to Mesozoic paleoceanography." *Chemical Geology* 324 (2012): 46-58.

Tribovillard, Nicolas, Philippe Récourt, and Alain Trentesaux. "Bacterial calcification as a possible trigger for francolite precipitation under sulfidic conditions." *Comptes Rendus Geoscience* 342.1 (2010): 27-35.

Tuovinen, Hanna, et al. "A comparison of analytical methods for determining uranium and thorium in ores and mill tailings." *Journal of Geochemical Exploration* 148 (2015): 174-180.

Turner, Adam C.E. “δ15N excursion in the Heebner shale: significance for the duration of post-glacial transgressions in the Late Pennsylvanian Midcontinent Sea.” *GSA South-Central Section - 49th Annual Meeting (19–20 March 2015).*

Usero, J., et al. "Comparative study of three sequential extraction procedures for metals in marine sediments." *Environment International* 24.4 (1998): 487-496.

Vaimakis, Tiberius C., and Evangelos D. Economou. "Evaluation of the mechanism of Greek calcareous phosphate ore dissolution by acetic acid solutions by X-ray powder diffraction and thermal analyses." *Industrial & engineering chemistry research* 37.11 (1998): 4306-4313.

Vandenbroucke, M., and C. Largeau. "Kerogen origin, evolution and structure."*Organic Geochemistry* 38.5 (2007): 719-833.

Watney, W. Lynn. "Gamma ray-neutron cross-plots as an aid in sedimentological analysis." *Geomathematical and petrophysical studies in sedimentology, computers and geology* 3 (1979): 81-100.

Wenzel, Walter W., et al. "Arsenic fractionation in soils using an improved sequential extraction procedure." *Analytica Chimica Acta* 436.2 (2001): 309-323.

Wersin, Paul, et al. "Interaction between aqueous uranium (VI) and sulfide minerals: spectroscopic evidence for sorption and reduction." *Geochimica et Cosmochimica Acta* 58.13 (1994): 2829-2843.

Weyer, S., et al. "Natural fractionation of 238 U/235 U." *Geochimica et Cosmochimica Acta* 72.2 (2008): 345-359.

Wignall, Paul B., and James R. Maynard. "The sequence stratigraphy of transgressive black shales." *Source Rocks in a Sequence stratigraphic framework* 37 (1993): 35-47.

Xu, Guangping, et al. "Digestion methods for trace element measurements in shales: Paleoredox proxies examined." *Chemical Geology* 324 (2012): 132-147.

Yang, Wan, Michael Bruemmer, and Monica Turner-Williams. "Stratigraphic Architecture and Processes Controlling Coeval Deltaic, Platform Carbonate, and Condensed Shelf Sedimentation, Upper Pennsylvanian, Leavenworth Limestone-Heebner Shale-Plattsmouth Limestone-Heumader Shale Minor Cyclothem, SE Kansas and NE Oklahoma." (2003).

Yang, Yu, et al. "Impact of natural organic matter on uranium transport through saturated geologic materials: from molecular to column scale." *Environmental science & technology* 46.11 (2012): 5931-5938.

Zangerl, Rainer, Eugene Stanley Richardson, and Bertram G. Woodland. *The paleoecological history of two Pennsylvanian black shales*. Chicago Natural History Museum, 1963.

Zerbe, J., et al. "Speciation of heavy metals in bottom sediments of lakes. "*Polish Journal of Environmental Studies* 8 (1999): 331-340.

Zhang, Gengxin, et al. "Microbial reduction of chlorite and uranium followed by air oxidation." *Chemical Geology* 283.3 (2011): 242-250.

Zheng, Yan, et al. "Remobilization of authigenic uranium in marine sediments by bioturbation." *Geochimica et Cosmochimica Acta* 66.10 (2002): 1759-1772.

APPENDICES

APPENDIX A: ADDITIONAL ICP-MS DATA

Table 6: Additional trace metal data from the bulk microwave digestion of the Heebner samples. All values in ppm; values that were below detection limits are listed as an "x".

SAMPLE	51V	52Cr	59Co	60Ni	63Cu	66Zn	97Mo	111Cd	238U
S6	0.01	0.21	4.54	4.15	0.73	23.69	X	0.13	0.29
S8	0.01	1.26	0.15	0.04	2.50	X	0.03	0.01	0.81
S10	0.01	0.55	4.36	4.12	1.34	55.24	0.01	0.23	0.64
S12	0.01	0.55	0.11	0.22	1.92	X	0.01	0.03	0.63
S14	0.01	0.66	3.47	6.60	0.93	105.44	0.03	0.31	0.62
S16	0.01	0.93	3.09	7.02	1.41	122.25	0.02	0.41	0.75
S18	0.01	0.81	0.93	0.39	0.94	6.33	0.02	0.13	0.62
S22	0.01	0.58	0.86	1.06	0.34	28.48	0.01	0.29	0.16
C11	0.03	0.83	3.34	54.76	9.96	755.09	0.03	3.34	1.43
C12	0.01	0.85	0.20	3.12	3.15	66.18	0.02	0.44	1.49
C13	0.21	1.00	1.12	30.81	7.76	1653.03	0.52	71.03	1.06
C16	0.41	0.91	0.03	X	1.12	X	0.66	0.27	1.62
C18	0.58	1.35	1.05	17.11	2.12	1159.39	0.35	76.50	1.18
C20	0.26	1.11	0.44	3.45	0.02	168.20	0.11	13.96	1.36
C28	0.35	0.88	0.45	3.12	-0.13	13.83	0.52	1.53	0.57
C36	0.05	0.56	0.16	1.91	0.57	X	0.04	0.07	0.08
I82	1.53	2.42	4.07	21.87	5.10	889.74	0.37	35.76	2.53
I83	0.22	1.26	0.07	0.01	2.45	X	0.77	0.81	4.42
I85	0.22	1.47	2.80	35.52	7.47	1211.51	0.20	45.05	2.21
I86	0.71	2.00	2.70	29.43	8.20	861.58	0.80	57.57	1.64
I88	0.30	2.17	2.29	30.69	6.21	2168.39	0.57	79.47	1.27
I90	0.01	0.89	0.99	16.32	1.09	342.21	0.01	3.68	2.17
I92	0.04	1.74	0.11	2.48	3.15	X	0.02	1.18	0.94
I100	0.01	0.62	2.82	7.11	3.49	X	0.01	0.03	0.66

Table 7: Additional trace metal data from the E3 extracts of the Heebner samples

SAMPLE	51V	52Cr	59Co	60Ni	63Cu	66Zn	97Mo	111Cd	238U
S6	1.69	0.13	3.73	3.17	2.29	X	0.04	0.06	0.15
S8	3.84	2.52	0.21	0.24	9.10	X	1.00	0.02	0.28
S10	1.73	0.67	2.84	5.21	7.28	33.05	0.40	0.08	0.77
S12	1.56	0.89	0.36	0.90	5.45	23.21	0.24	0.10	0.26
S14	1.22	0.39	1.44	5.22	5.52	X	0.34	0.10	0.63
S16	1.95	1.41	1.89	7.15	7.81	X	0.45	0.29	2.47
S18	1.28	1.27	0.54	0.82	3.88	29.08	0.08	0.16	0.28
S22	0.79	0.60	0.78	2.61	6.98	92.80	0.04	0.22	0.16
C11	3.03	0.38	2.50	43.38	40.03	311.61	1.14	2.52	9.89
C12	3.10	1.28	0.37	5.36	22.46	103.62	0.63	0.53	1.26
C13	12.63	0.94	0.98	45.56	26.59	914.02	6.49	8.66	0.51
C16	39.50	9.10	0.72	0.11	25.98	X	7.26	9.99	33.84
C18	42.18	3.90	1.04	34.45	31.35	535.34	6.28	28.96	23.67
C20	31.12	10.40	0.67	11.82	20.17	139.33	1.77	17.65	45.94
C28	12.86	4.20	1.73	31.67	9.42	49.12	1.66	8.32	20.95
C36	2.30	1.32	0.90	18.42	13.65	X	0.09	0.28	0.37
I82	53.84	3.29	2.68	40.34	39.91	801.85	19.12	13.65	41.09
I83	49.49	6.10	0.44	3.47	11.51	X	17.63	8.07	30.66
I85	24.35	1.03	1.66	39.59	36.54	949.55	10.43	10.59	1.13
I86	28.17	2.11	1.78	37.48	36.28	833.43	8.06	13.45	0.80
I88	46.73	2.12	1.79	39.29	49.57	1213.82	14.82	15.89	0.88
I90	12.81	1.74	2.09	19.84	19.95	378.94	0.69	3.14	1.74
I92	14.68	4.19	0.24	7.41	30.76	5.17	0.78	2.62	1.12
I100	2.02	0.91	3.51	12.74	10.68	X	0.41	X	0.80

Table 8: Additional trace metal data from the E4 extracts of the Heebner samples

SAMPLE	51V	52Cr	59Co	60Ni	63Cu	66Zn	97Mo	111Cd	238U
S6	3.53	3.31	5.30	29.88	9.84	345.85	0.10	1.13	0.37
S8	12.39	8.61	5.22	64.73	19.49	116.62	3.35	0.36	0.81
S10	12.41	16.64	5.98	87.37	22.10	229.09	2.98	1.11	0.98
S12	13.31	13.45	3.16	67.77	22.01	241.36	1.23	1.06	0.72
S14	13.30	18.82	3.77	77.64	26.68	270.34	4.13	1.84	0.53
S16	10.62	20.76	3.55	94.21	30.69	291.66	2.49	0.96	0.83
S18	10.76	14.16	3.23	68.03	13.61	111.62	2.52	0.42	0.56
S22	9.41	15.72	3.27	85.55	14.86	230.45	1.61	0.61	0.70
C11	17.87	27.80	8.17	169.60	57.69	357.95	10.88	2.79	2.74
C12	42.62	31.63	5.48	118.13	45.90	542.05	25.31	5.32	2.57
C13	126.91	27.56	5.46	136.62	47.52	3942.87	139.89	92.28	2.42
C16	98.18	25.85	1.82	50.70	20.98	101.88	56.57	1.87	3.10
C18	179.33	38.94	4.72	112.60	47.48	606.70	83.69	27.97	3.52
C20	86.71	44.87	2.62	74.94	32.96	126.42	40.99	6.88	7.49
C28	63.33	62.11	5.00	135.90	35.51	154.97	24.14	3.74	8.83
C36	19.13	36.73	6.38	123.78	25.52	43.59	4.06	0.26	1.47
I82	111.66	14.52	3.72	81.74	23.25	715.52	64.71	22.73	4.08
I83	173.95	22.57	3.55	95.40	21.57	276.98	140.75	2.79	5.01
I85	146.94	25.84	4.48	113.43	32.29	1393.84	153.97	33.11	2.27
I86	176.62	35.56	4.62	125.60	37.01	1773.10	115.22	58.66	2.52
I88	324.69	44.02	6.35	201.29	49.67	1534.63	276.04	44.28	2.57
I90	139.59	29.05	4.64	107.90	26.57	389.97	78.33	5.87	2.72
I92	303.82	82.21	4.69	217.92	47.82	206.50	150.46	5.23	5.87
I100	4.01	7.41	3.88	38.84	13.15	X	0.93	0.01	0.67

Table 9: Additional trace metal data from the E5 extracts of the Heebner samples

SAMPLE	51V	52Cr	59Co	60Ni	63Cu	66Zn	97Mo	111Cd	238U
S6	25.08	19.08	4.62	16.27	5.73	1173.81	1.23	3.28	0.52
S8	49.09	37.79	3.13	11.31	10.8	19.22	10.55	0.12	1.25
S10	26.17	39.8	4.67	15.4	7.94	96.38	3.2	0.37	1.2
S12	32.95	42.6	4.14	13.69	10.45	176.98	1.56	0.4	0.83
S14	33.33	58.84	4.22	15.31	12.34	57.11	1.77	0.11	1.25
S16	28.02	52.95	4.42	16.23	12.59	129.57	3.57	0.26	1.09
S18	39.8	63.18	2.98	8.87	3.96	78.42	2.45	0.01	1.21
S22	21.25	48.65	2.33	11.9	13.02	222.6	2.21	0.19	0.68
C11	29.76	83.83	1.85	6.97	20.56	23.56	2.34	0.25	1.64
C12	88	136.66	1.32	6.65	27.92	126.35	4.63	0.62	1.8
C13	252.13	83.2	1.27	6.95	9.09	172.07	5.71	1.4	2.14
C16	342.15	139.36	1.39	13.57	22.15	215.16	25.41	0.35	1.68
C18	368.07	111.44	1.78	8.75	10.34	69.63	7.99	1.09	1.62
C20	335.51	224.61	2.3	31.79	14.5	528.46	52.44	1.24	1.78
C28	105.28	156.68	3.53	34.76	30.11	357.84	25.43	0.26	1.86
C36	27.4	95.53	4.27	13.94	22.43	65.98	1.21	0.05	0.67
I82	X	56.45	4.04	15.75	9.27	213.65	31.86	1.06	3.29
I83	938.44	154.78	2.12	15.3	22.55	266.76	67.68	0.93	5.45
I85	534.43	106.24	4.71	19.23	7.71	195.36	41.38	1.28	4.97
I86	564.98	138.25	3.46	11.7	5.81	184.85	17.97	1.75	4.37
I88	844.21	161.82	2.18	9.66	11.74	176.4	13.7	1.94	4.9
I90	543.43	141.9	4.51	33.37	30.8	318.15	72.38	1.23	5.11
I92	449.72	234.55	1.11	8.63	22.65	193.43	29.66	0.29	2.69
I100	21.66	31.01	5.4	21.93	10.52	14.16	5.71	0.01	0.66

Table 10: [U] of Heebner extracts; standard addition calibration

SAMPLE	E1	E2	E3	E4	E5	TOTAL
S6	X	0.24	0.19	0.51	0.52	1.46
S6*	X	0.23	0.23	0.30	0.64	1.41
S8	0.82	0.78	0.35	0.70	1.20	3.85
S10	0.18	0.49	0.71	0.88	1.12	3.37
S12	0.05	0.63	0.37	0.65	0.82	2.51
S14	0.14	0.56	1.31	0.46	1.21	3.67
S16	0.03	0.71	2.37	0.82	1.13	5.07
S18	X	0.44	0.56	0.52	0.97	2.50
S22	X	0.20	0.16	0.60	0.95	1.91
C11	X	1.04	9.35	1.78	1.65	13.82
C12	X	1.56	1.66	2.34	1.63	7.19
C13	0.27	1.00	0.70	2.09	2.04	6.09
C16	X	1.80	20.98	2.56	1.80	27.15
C18	0.43	1.13	25.43	3.07	1.46	31.52
C20	1.12	1.79	62.36	6.73	1.41	73.41
C28	X	0.50	23.18	7.98	2.09	33.75
C36	X	0.14	0.32	1.14	0.71	2.31
I82	0.24	1.07	36.67	3.54	3.33	44.85
I83	0.07	3.62	37.64	4.22	5.62	51.17
I85	0.26	1.68	1.01	2.09	5.25	10.30
I86	0.28	1.55	0.81	2.28	3.90	8.82
I88	0.32	1.23	0.95	2.50	4.59	9.60
I90	X	2.25	2.00	2.71	6.98	13.94
I92	X	0.86	1.20	6.37	2.45	10.89
I100	0.09	0.64	0.64	0.62	0.67	2.66

Table 11: [U] of microwave-digested bulk Heebner samples; external calibration

Sample	238U
S6	n/d
S8	8.35
S10	6.58
S12	4.07
S14	5.32
S16	7.52
S18	4.58
S22	2.52
C11	21.24
C12	9.59
C13	9.10
C16	34.27
C18	43.94
C20	102.21
C28	46.55
C36	3.54
I82	62.56
I83	67.14
I85	n/d
I86	12.46
I88	13.46
I90	15.20
I92	13.86
I100	4.49
SBC-1	2.63

APPENDIX B: TABULATED XRD DATA AND DIAGRAMS

Table 12: Estimated mineral weight percentages for the Heebner samples. S = Sedan samples, C = Clinton, I = I229

Sample	Quartz	Total Clay	Dolomite	Calcite	Pyrite	Plagioclase	Apatite
S6	53.4	31.6	0.9	4.1	2	7.1	0.9
S8	54.3	33.5	0	0.9	3.2	7.3	0.8
S10	55	24.5	0.3	6.4	1.6	12.3	0
S12	52.4	33	0.6	0	1.5	11.5	1
S14	55.9	26.2	0.4	3.5	1.8	11.2	1.1
S16	56.9	26	0.5	0	1.9	13.3	1.4
S18	63.3	25.2	0.4	0	0	10.2	0.9
S22	66.4	23.7	0.4	0	0	8.8	0.7
C11	48.4	33.8	1.6	1	2.2	9.1	4
C12	47.7	41.3	0	0	0	11	0
C13	48.9	21.8	5.6	14.4	4.7	4.6	0
C16	50.1	32.5	0	0	0	5.2	12.2
C18	44.9	25.2	4.4	7.2	3.4	8.4	6.7
C20	42.2	19.1	4	5	0	7.1	22.6
C28	53.2	28.1	0	0	0	7.6	11.2
C36	58.5	31.1	0	0	0	10.4	0

(Table 12 continued)

I82	49.4	22.8	2.5	4.9	1.3	14.3	4.8
I83	44.8	39.3	0	0	0	8.8	7.2
I85	51.9	22.7	3.5	3.2	2.7	15	1
I86	49	24.2	5.1	4.5	2.3	14.9	0
I88	44.3	26.5	7.8	4.4	4.6	11.7	0.8
I90	57.8	26.5	0	0	1	13.7	1
I92	50.2	38.8	0	0	1.5	9.4	0
I100	56.1	23.5	1.8	0	1.1	17.1	0.4

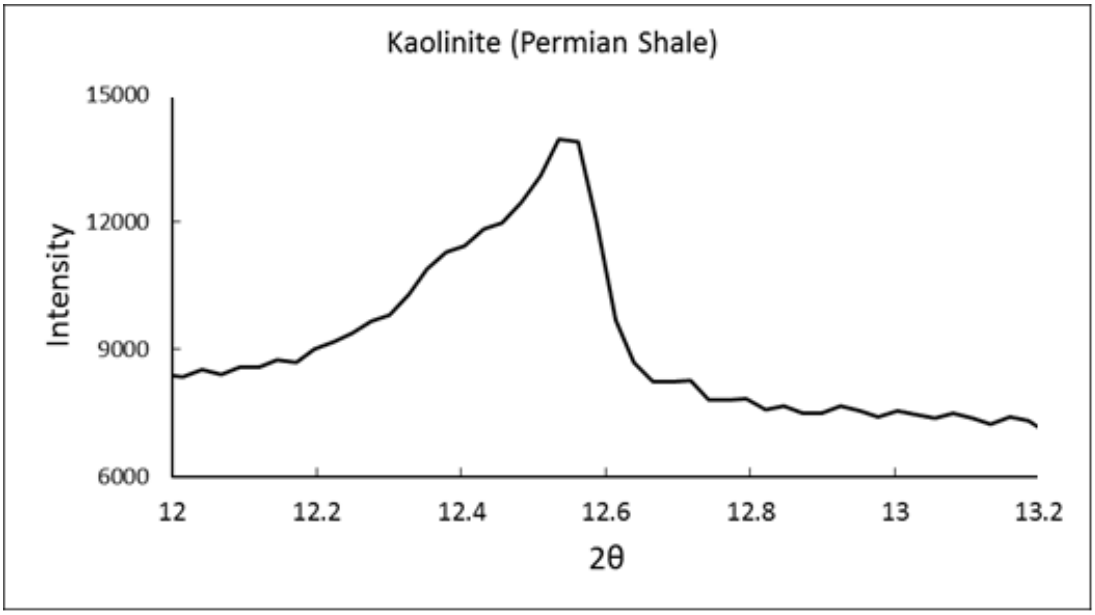

Figure 19: Diagnostic kaolinite peak for the Permian cyclothem shale.

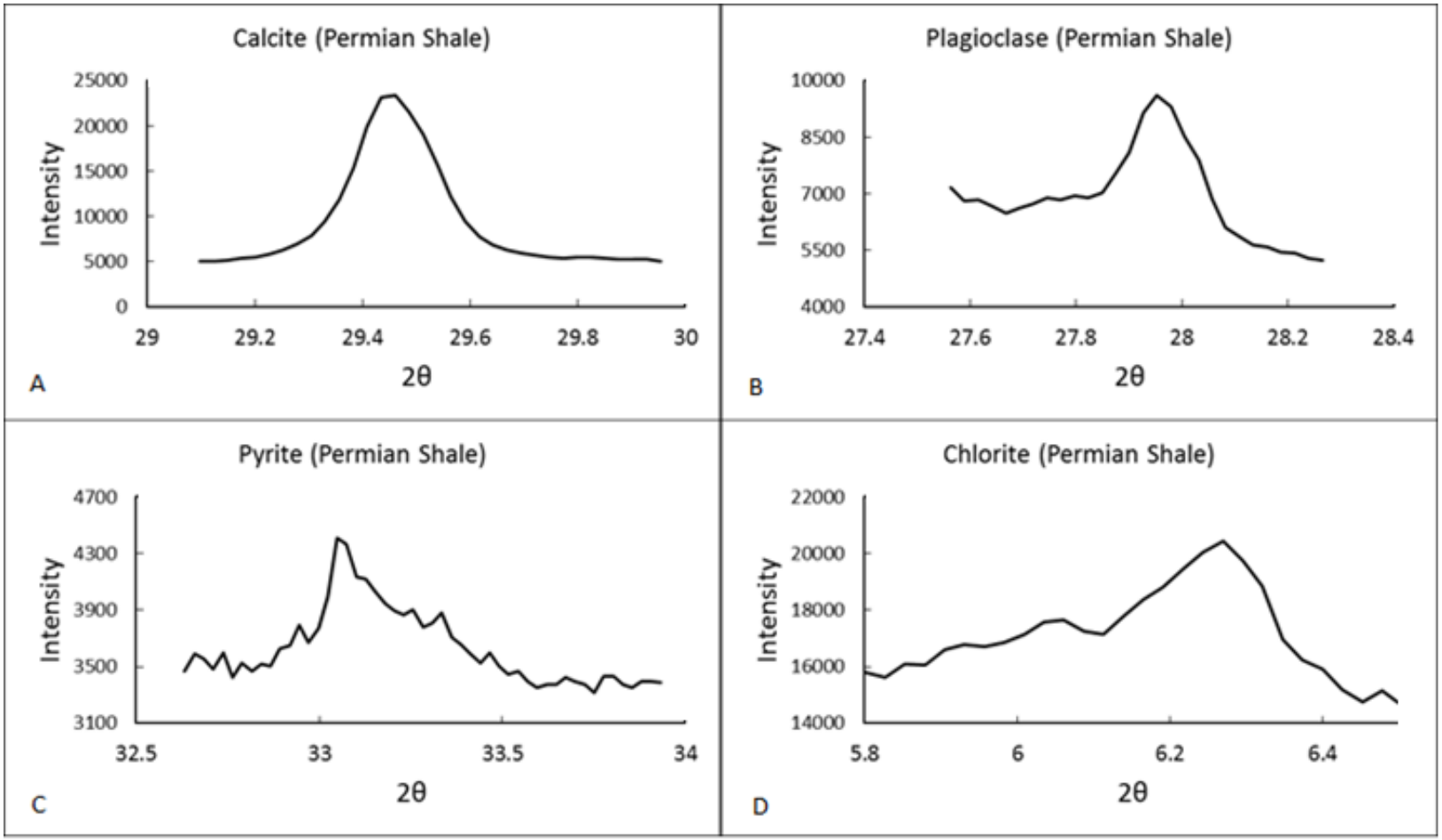

Figure 20: Diagnostic peaks for calcite, plagioclase, pyrite, and chlorite for the Permian cyclothem shale.

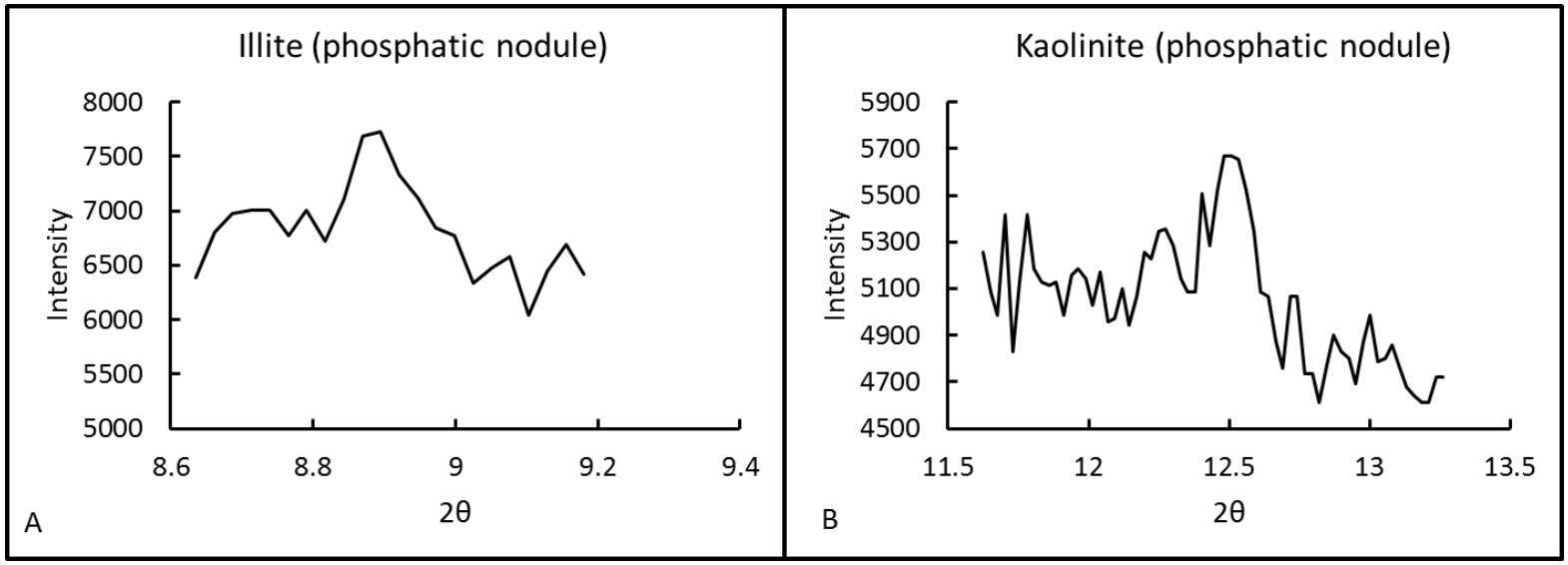

Figure 21: Diagnostic peaks for illite and kaolinite in the phosphatic nodule.

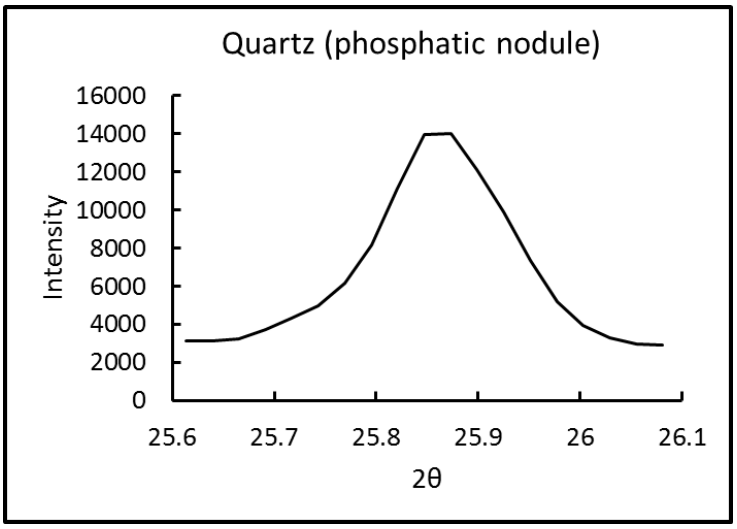

Figure 22: Diagnostic peak for quartz in the phosphatic nodule.

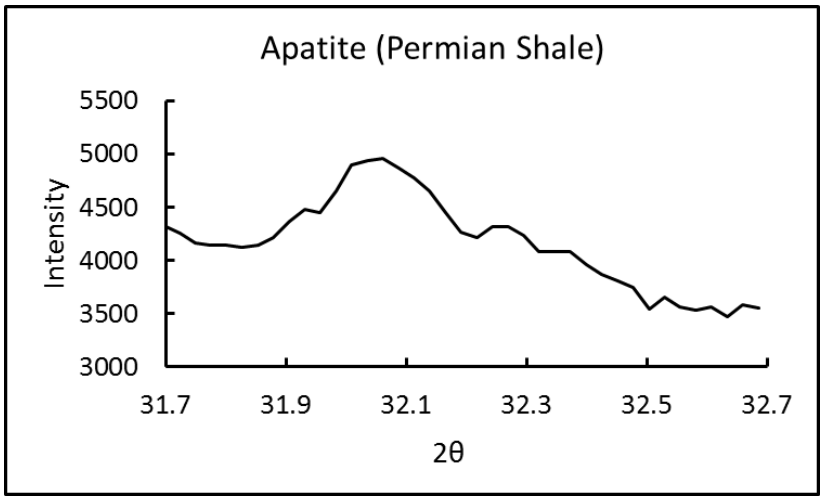

Figure 23: Diagnostic peak for apatite in the Permian cyclothem shale.

APPENDIX C: ADDITIONAL BACKGROUND INFORMATION

THE $\delta^{238}U$ PALEOREDOX PROXY

The $\delta^{238}U$ value of a particular sediment appears to be dependent on the prevailing redox conditions of its deposition. Sediments deposited under reducing conditions generally tend to show positive (^{238}U enriched) $\delta^{238}U$ values (Murphy 2013, Weyer et al. 2008, Andersen et al. 2014, Noordman et al. 2015, Holmden et al. 2015). Enrichment of the heavier isotope defies traditional mass-dependent interpretations, and is thought to be a consequence of the "nuclear volume effect", where mass-dependent fractionation is superseded by volume-dependent effects (Schauble 2007, Bopp et al. 2010). The lightest $\delta^{238}U$ values (^{235}U enriched) are seen in sediments deposited under oxic conditions, with suboxic conditions intermediate (Weyer et al. 2008, Goto et al. 2014). Given this trend, $\delta^{238}U$ could potentially be used as a sliding scale indicator of redox state.

The long residence time, uniform concentration, and stable isotopic composition of U in the modern ocean (Brennecka et al. 2008, Stirling et al. 2007, Andersen et al. 2015) suggests that it may be suitable as a global-scale paleoredox proxy. The U isotopic composition of the ocean is the result of the interplay between its ultimate source in the continental crust and its ultimate sinks within different types of marine sediments.

In the modern oxygenated ocean, suboxic and oxic sediment sinks are estimated to account for approximately 90% of U removal, while anoxic and euxinic sinks comprise the remainder (Brennecka et al. 2011). However, the relative size of these sinks has likely varied through geologic time - sometimes substantially, as evidenced by periods of widespread black shale deposition (Piper & Calvert 2009). An increase in the prevalence of global anoxic sinks should correlate to a trending decrease in U concentration and a lighter isotopic signal in marine deposits due to an intensification of ^{238}U removal. If the isotopic input from the continental crust to the oceans is assumed constant, the δ^{238} of the marine rock record through time are then a function of the size of its various sinks, which can be estimated through mass balance equations (Brennecka et al. 2011, Montoya-Pino et al. 2010, Goto et al. 2014).

The δ^{238} paleoredox proxy has been tested against several known global disturbances such as the end-Permian extinction (Brennecka et al. 2011), Archean oxidation events (Kendall et al. 2013), the post-Great Oxygenation Shunga Event (Asael et al. 2013), the Steptoean Positive Carbon Isotope Excursion (SPICE) (Dahl et al. 2014), the ocean oxygenation event of the late Edicarian (Kendall et al. 2015), and the Ocean Anoxic Event 2 (OAE2) (Montoya-Pino). The application of $\delta^{238}U$ has thus far has been promising, and there are several areas of active research that seek to better understand the fundamental processes at work.

The precise mechanism(s) of fractionation in anoxic sediments is unclear. Several recent studies have implicated the role of bacterial reduction in ^{238}U enrichment (Stirling et al. 2015, Stylo 2015, Basu et al. 2014). Stylo et al. 2015 tested the isotopic signatures of abiotic reduction using reductants such as magnetite, aqueous Fe(II), FeS, aqueous sulfide, and peat. They also

tested the signature of bioreduction via a metal-reducing bacterium (*Shewanella oneidensis).* While the rates of reduction were fairly similar, the abiotic modes of reduction exhibited a negligible fractionation between the dissolved pool and solid phase, and the biotic reduction induced a larger (^{238}U-enriched) signature. In the biotic experiments, the dissolved pool showed a ~-2 per mille fractionation in accordance with a preferential uptake of U^{238} by the bacterially-reduced solids. Moreover, they found that the fractionation due to biotic reduction was specifically the result of enzymatic electron transfer rather than uptake of U^{VI} across the outer cellular membrane. Similar values of $^{238}U/^{235}U$ fractionation have been reported for other metal-reducing bacteria by Basu et al. 2014.

Andersen et al. 2014 posited that the U-isotope composition of anoxic sediments is affected by diffusion from the water column and reaction processes within the sediments – namely pore water chemistry, detrital contribution, sedimentation rates, and authigenic U accumulation. An important consideration outlined by Andersen et al. (2014) is the influence of reservoir effects and oxygen penetration depth on U isotope composition. A restricted marine basin with anoxic or euxinic conditions in and above the sediment would display a sharp gradient towards high $\delta^{238}U$ values, but as the water column reservoir is depleted the values would become progressively lighter. This is in contrast to an open marine setting, where any recorded drawdown would be related to global conditions and not a local effect. Anoxic sediments under a suboxic or oxic water column would display lighter values due to a lengthening of the diffusive pathway (seawater U to reducing pore waters). A final scenario postulated by Andersen et al. 2014 suggests that partial U-reduction in the pore water (in a suboxic or anoxic setting) would lead to a lower overall concentration of U and a shallow $\delta^{238}U$ gradient in the sediment, but higher bulk $\delta^{238}U$ values due to mass balance constraints. The influence of sedimentation rates and reservoir effects has also been demonstrated by $\delta^{238}U$ studies in the Baltic Sea and Kyllaren Fjord (Noordman et al. 2015).

The fractionation associated with carbonate material is also an active area of research. Primary precipitates appear to record the $\delta^{238}U$ of contemporaneous seawater (Weyer et al. 2008, Romaniello et al. 2013), and may provide a direct proxy for ocean chemistry reconstructions. Work by Romaniello et al. 2013 has shown that bulk carbonate sediments can display a greater range of values, and do not record seawater values as faithfully as primary precipitates.

APPENDIX D: METHODOLOGY DETAILS

All reactions for the sequential extractions were carried out in 50ml polyethylene centrifuge tubes. During the reaction periods, the tubes were kept in a horizontal agitation chamber set to 150rpm and 25°C. The solid material would eventually settle and required periodic shaking by hand to ensure even exposure to the reagent. After each reaction step, the tubes were centrifuged for 15 minutes and the supernatants were extracted with a pipette and transferred into separate 50ml centrifuge tubes. After the removal of the supernatant 7mls of 18MΩ deionized water was added into each reaction tube, which were then shaken by hand until all solid matter was disaggregated and in suspension. The tubes were centrifuged again and the wash water was pipetted into the first extracted supernatant. This washing procedure

was repeated verbatim a second time to ensure the complete removal of the prior reagent for the next extraction step. Before aliquots of the stock solutions were taken for dilution and ICP-MS analysis, the stock solutions were allowed to sit (typically for several days) to allow for any small particles to settle. Care was taken during the addition of hydrogen peroxide to the samples; the reaction can be significantly delayed and so each full aliquot of the reagent was added slowly over the course of an hour. For the Heebner samples, multiple aliquots of H_2O_2/HNO_3 were added (and centrifuged and pipetted out) until effervescence was muted. During the ashing of black shale samples, several tests suggested that an unidentified new U-bearing phase (an oxide?) is formed that is insoluble in mild extractive reagents such as $MgCl_2$.

VITA

Max Lindaman was born and raised on Long Island, New York. His interest in geology is rooted in a general appreciation of nature and from numerous family excursions to the forests of upstate New York, where the streambeds expose some good fossils (if you look hard enough). This interest was reignited upon taking earth science electives at Stony Brook University, where he would go on to get a B.S. in Geology.

After a brief hiatus from academia, Max left for Baton Rouge with a small army of musical instruments to obtain a Master's degree at Louisiana State University with a focus on uranium geochemistry. As of graduation, Max is currently working for the U.S. Geological Survey in Baton Rouge assisting with groundwater studies.